nature metabolism

ARTICLES

https://doi.org/10.1038/s42255-019-0098-8

Oncogenic Rag GTPase signalling enhances B cell activation and drives follicular lymphoma sensitive to pharmacological inhibition of mTOR

Ana Ortega-Molina[1], Nerea Deleyto-Seldas[1], Joaquim Carreras[2], Alba Sanz[1], Cristina Lebrero-Fernández[1], Camino Menéndez[1], Andrew Vandenberg[1], Beatriz Fernández-Ruiz[1], Leyre Marín-Arraiza[1], Celia de la Calle Arregui[1], Ana Belén Plata-Gómez[1], Eduardo Caleiras[3], Alba de Martino[3], Nuria Martínez-Martín[4], Kevin Troulé[5], Elena Piñeiro-Yáñez[5], Naoya Nakamura[2], Shamzah Araf[6], Gabriel D. Victora[7], Jessica Okosun[6], Jude Fitzgibbon[6] and Alejo Efeyan[1]*

The humoral immune response requires that B cells undergo a sudden anabolic shift and high cellular nutrient levels, which are required to sustain the subsequent proliferative burst. Follicular lymphoma (FL) originates from B cells that have participated in the humoral response, and 15% of FL samples harbour point-activating mutations in *RRAGC*, an essential activator of mTORC1 downstream of the sensing of cellular nutrients. The impact of recurrent *RRAGC* mutations in B cell function and lymphoma is unexplored. *RRAGC* mutations, targeted to the endogenous locus in mice, confer a partial insensitivity to nutrient deprivation, but strongly exacerbate B cell responses and accelerate lymphomagenesis, while creating a selective vulnerability to pharmacological inhibition of mTORC1. This moderate increase in nutrient signalling synergizes with paracrine cues from the supportive T cell microenvironment that activate B cells via the PI3K–Akt–mTORC1 axis. Hence, *Rragc* mutations sustain induced germinal centres and murine and human FL in the presence of decreased T cell help. Our results support a model in which activating mutations in the nutrient signalling pathway foster lymphomagenesis by corrupting a nutrient-dependent control over paracrine signals from the T cell microenvironment.

Follicular lymphoma is the second most frequent form of non-Hodgkin lymphoma and, in spite of its indolent nature, remains mostly incurable[1]. This lymphoma derives from B lymphocytes that have participated in germinal centres (GCs), transient anatomical structures formed primarily by B and T cells during the humoral response to infection and immunization[2]. The GC enables the production of high-affinity antibodies by iterative rounds of a two-step process consisting of affinity-based selection of antibody-producing B cells, which requires paracrine signals from follicular helper T (Tfh) cells, followed by proliferation and programmed mutation of the immunoglobulin locus in selected B cells[3–6]. Importantly, FL maintains a follicular architecture reminiscent of the GC, and non-B lymphocyte cellular components of the GC, including Tfh, are also present in the FL[7]. Ninety percent of FLs harbour a t(14;18) chromosome translocation that leads to the overexpression of the anti-apoptotic gene *BCL2* by placing it under the control of the immunoglobulin heavy chain enhancer[8]. Additional genetic alterations include mutations in the epigenetic regulators *KMT2D*, *CREBBP* and *EZH2* (refs. [9–13]), and genes involved in the interaction with the microenvironment of both FL and aggressive lymphoma, such as *TNFRSF14*, *B2M* and *CD58* (refs. [9,14–18]).

We and others have recently identified recurrent mutations in components of the nutrient sensing pathway[17,19–21] that activates the mechanistic target of rapamycin complex 1 (mTORC1), a serine/threonine kinase driver of cellular anabolism[22]. A large fraction of these missense mutations cluster within the nucleotide-binding domain of the gene encoding the RagC GTPase (also known as *RRAGC*), which forms a heterodimeric complex with RagA responsible for activating mTORC1 upon cellular nutrient sufficiency[23]. In the presence of cellular nutrients, such as certain amino acids, the Rag heterodimer acquires a specific nucleotide configuration that enables its interaction with mTORC1, leading to its recruitment to the outer lysosomal surface[24,25]. Importantly, ectopic expression of these mutant variants in cancer cell lines leads to increased recruitment and activation of mTORC1 (refs. [19,20,26]).

Independent of the cellular nutrient signals, growth factors and cytokines, including paracrine signals from Tfh to B cells, activate mTORC1 via the PI3K–Akt signalling cascade[27,28]. Mutations in the Rag GTPases are rare in other lymphoid and solid malignancies, arguing for a particular effect of such genetic alterations on the physiology and pathology of B lymphocytes. Although point mutations in either *RRAGC* or *RRAGA* can functionally activate the mTORC1 pathway[25,29], the reason for a selective genetic activation of *RRAGC*, sparing *RRAGA*, remains unclear.

We have engineered mouse strains that endogenously express RagC mutants, to address their oncogenic potential and to understand the physiological impact that nutrient signalling may have on normal and pathological B cell responses. These genetic tools

[1]Metabolism and Cell Signalling Laboratory, Spanish National Cancer Research Centre, Madrid, Spain. [2]School of Medicine, Department of Pathology, Tokai University, Isehara, Japan. [3]Histopathology Unit, Spanish National Cancer Research Centre, Madrid, Spain. [4]Centro de Biología Molecular Severo Ochoa, Madrid, Spain. [5]Bioinformatics Unit, Spanish National Cancer Research Centre, Madrid, Spain. [6]Centre for Haemato-Oncology, Barts Cancer Institute, Queen Mary University of London, London, UK. [7]Laboratory of Lymphocyte Dynamics, The Rockefeller University, New York, NY, USA.
*e-mail: aefeyan@cnio.es

accelerated experimental lymphomagenesis, while creating a vulnerability to mTORC1 inhibitors. Mutations in the nutrient signalling pathway enhanced B cell autonomous activation, corrupting a nutrient-dependent control of paracrine-positive signals from the T cell microenvironment.

Results

RagC knock-in mice show partial insensitivity to nutrient withdrawal. To determine the impact of mutations in the nutrient sensing pathway on B cell function and FL development in a physiological setting, we used CRISPR/Cas9 genome engineering[30] to generate two independent murine *Rragc* knock-in models carrying point mutations recurrently observed in human FL samples: S74C and T89N (Supplementary Fig. 1a), corresponding to S75C and T90N, respectively, in human RAGC protein[17,19–21]. The variant T90 was the most frequently observed[20], and S75 was mutated to at least three different amino acids (S75C, S75A, S75F); both mutants are likely to have functional consequences[26,29]. In addition to the amino acid change, we introduced additional silent mutations for diagnostic and genotyping purposes, and in the protospacer adjacent motive sequence to prevent retargeting (Supplementary Fig. 1b).

RagC$^{S74C/+}$ and RagC$^{T89N/+}$ mice were obtained with sub-Mendelian ratios (Supplementary Fig. 1c,d), suggesting that partially penetrant lethality occurs before weaning. Moreover, crossing heterozygous RagC$^{S74C/+}$ or RagC$^{T89N/+}$ yielded no viable homozygous E19.5 neonates. These findings were not surprising, as fully penetrant neonatal lethality was seen in mice endogenously expressing a constitutively active form of RagA (RagA^{Q66L} or RagA^{GTP})[31]. Surviving young, heterozygous RagC mutant mice showed no obvious phenotypic alterations. We tested whether the expression of RagC mutants in heterozygosity conferred insensitivity to cellular nutrient withdrawal in cultured mouse embryonic fibroblasts (MEFs). mTORC1 activity was only partially resistant to withdrawal of all amino acids in both RagC$^{S74C/+}$ and RagC$^{T89N/+}$ cultures, as revealed by phosphorylation of the mTORC1 targets T389-S6K and T37/46-4EBP1 (Fig. 1a, P-S6K1 quantified in Supplementary Fig. 1e, with additional quantification of independent experiments in Supplementary Fig. 1f). Importantly, compared with the maximal activity observed in wild-type cells, no supra-physiological increase in mTORC1 activity was seen in MEFs that endogenously expressed RagC mutant variants. Partial resistance to nutrient deprivation was more evident, albeit still incomplete, on withdrawal of either leucine or arginine (Fig. 1a), two key amino acids involved in Rag GTPase-mediated activation of mTORC1 (refs. [32,33]). As expected, phosphorylation of Akt at Ser 473 and Thr 308, which occurs independently of the activation of the nutrient signalling cascade but depends on growth factor signalling, is unaffected in RagC mutant cells (Fig. 1a). In time-lapse experiments, as in ref. [26], we observed that RagC mutants delayed the deactivation of mTORC1 by amino acid withdrawal (Fig. 1b). Partial reactivation of the pathway by extended amino acid withdrawal was probably a consequence of the autophagic degradation of internal cellular storages that occurs on mTORC1 inhibition, as addition of chloroquine to starved cells prevented partial reactivation of mTORC1 (Supplementary Fig. 1g).

We next evaluated whether naïve B lymphocytes purified from RagC mutant mice (Fig. 1c) also showed nutrient-independent mTORC1 activity. In the absence of a growth factor-like stimulus and amino acids in the medium, mTORC1 activity was very low and comparable to the level of rapamycin-treated samples, as revealed by the intracellular immunostaining for phosphorylated serines 235/236 of S6 (Fig. 1d). Without amino acids in the medium, stimulation with ligands that mimic paracrine-activating signals from T cells that stimulate mTORC1 via PI3K–Akt (IL-4 and an anti-CD40-activating antibody) resulted in greater stimulation of mTORC1 activity in RagC$^{S74C/+}$ and RagC$^{T89N/+}$ B cells compared with RagC$^{+/+}$ cells (Fig. 1d). Simultaneous addition of amino acids and cytokines further activated mTORC1 activity in all cells, indicating that, as in MEFs, the presence of amino acids was only partially dispensable for mTORC1 activation in the mutant B cells. For a comparison, we performed these signalling experiments side-by-side with B cells expressing the tool RagA^{GTP} (Q66L) mutation in heterozygosity and homozygosity. We have previously shown[31] that mTORC1 in MEFs and neonatal tissues from RagA$^{GTP/GTP}$ mice was completely insensitive to nutrient starvation; this was also evident in RagA$^{GTP/GTP}$ B lymphocytes (Fig. 1d). Heterozygous RagA$^{GTP/+}$ cells, in contrast to RagC$^{S74C/+}$ and RagC$^{T89N/+}$ cells, showed no detectable signalling perturbation (Fig. 1d and ref. [31]). The partial resistance to amino acid, leucine and arginine withdrawal was also observed in whole-protein extracts from stimulated B cells (Fig. 1e). Collectively, these results show that RagC mutations, when expressed endogenously and in heterozygosity, have a modest but significant activating effect on the regulation of mTORC1 by nutrients, while the presence of an activating mutation in RagA in heterozygosity is inconsequential. These data, generated without relying on the limitations of heterologous expression systems, provide cellular evidence for a biochemical asymmetry of the Rag heterodimeric components toward the control of mTORC1 activation, and are consistent with previous in vitro studies[26]. In addition, they provide a potential explanation for the exclusive occurrence of *RRAGC* heterozygous mutations, and the absence of mutations in *RRAGA* in human FL.

Because the expression of the point-mutant RagC variants is not restricted to B lymphocytes, we next quantified the proportions of different populations of the haematopoietic lineage, to exclude potential consequences of the expression of these variants in non-B cell populations. Lymphoid (B cells, CD4$^+$ and CD8$^+$ T cells) and myeloid (granulocytes, macrophages, myeloid cells and myeloid-derived suppressor cells) populations were present in RagC mutant mice in frequencies similar to those of wild-type counterparts, in both spleen and bone marrow (BM) (Supplementary Fig. 1h). Hence, while these quantifications are not a thorough functional examination of all populations in the haematopoietic lineage, it is apparent that the endogenous expression of RagC mutations has no obvious effect on lymphoid and myeloid lineages that could complicate further functional studies on B cells.

RagC mutations accelerate FLs that are sensitive to rapamycin. We next bred RagC mutant S74C and T89N strains with the transgenic mouse strain VavP-Bcl2, which expresses Bcl2 under the lymphoid lineage-specific promoter VavP (VavP-Bcl2^{tg}), the standard genetic tool to generate autochthonous FL in mice[34]. The partial insensitivity to amino acid withdrawal observed in RagC mutant B cells was also observed in the VavP-Bcl2 background (Supplementary Fig. 2a). Latencies to lymphoma development of VavP-Bcl2^{tg}; RagC$^{S74C/+}$ and VavP-Bcl2^{tg}; RagC$^{T89N/+}$ mice were significantly accelerated (Fig. 2a), which was also true for BM chimeras (Supplementary Fig. 2b). Murine FLs were diagnosed by pathognomonic histological features of FL, such as expression of Bcl6 in spleen and lymph nodes, indicating that these tumours were of GC B cell origin (Fig. 2b). Histological analysis of lymphoid organs from FL-bearing mice of all three genotypes revealed similar incidence (Fig. 2c) and spread (Supplementary Fig. 2c,d). Lymphoma incidence and spread were also similar in all three genotypes when complete cohorts of mice were euthanized at 250 days (Fig. 2d and Supplementary Fig. 2e).

Of note, VavP-Bcl2 mice were also prone to develop autoimmunity[34], so their limited overall survival was due to occurrence of FL and/or autoimmune disease. To our surprise, in addition to the acceleration of FL development, we observed that VavP-Bcl2^{tg}; RagC$^{S74C/+}$ and VavP-Bcl2^{tg}; RagC$^{T89N/+}$ mice and BM chimeras also exhibited shortened latency to autoimmunity (Supplementary Fig. 2f). Consistent with the acceleration of both prevalent pathologies in VavP-Bcl2 mice, overall survival (including lymphoma-free and

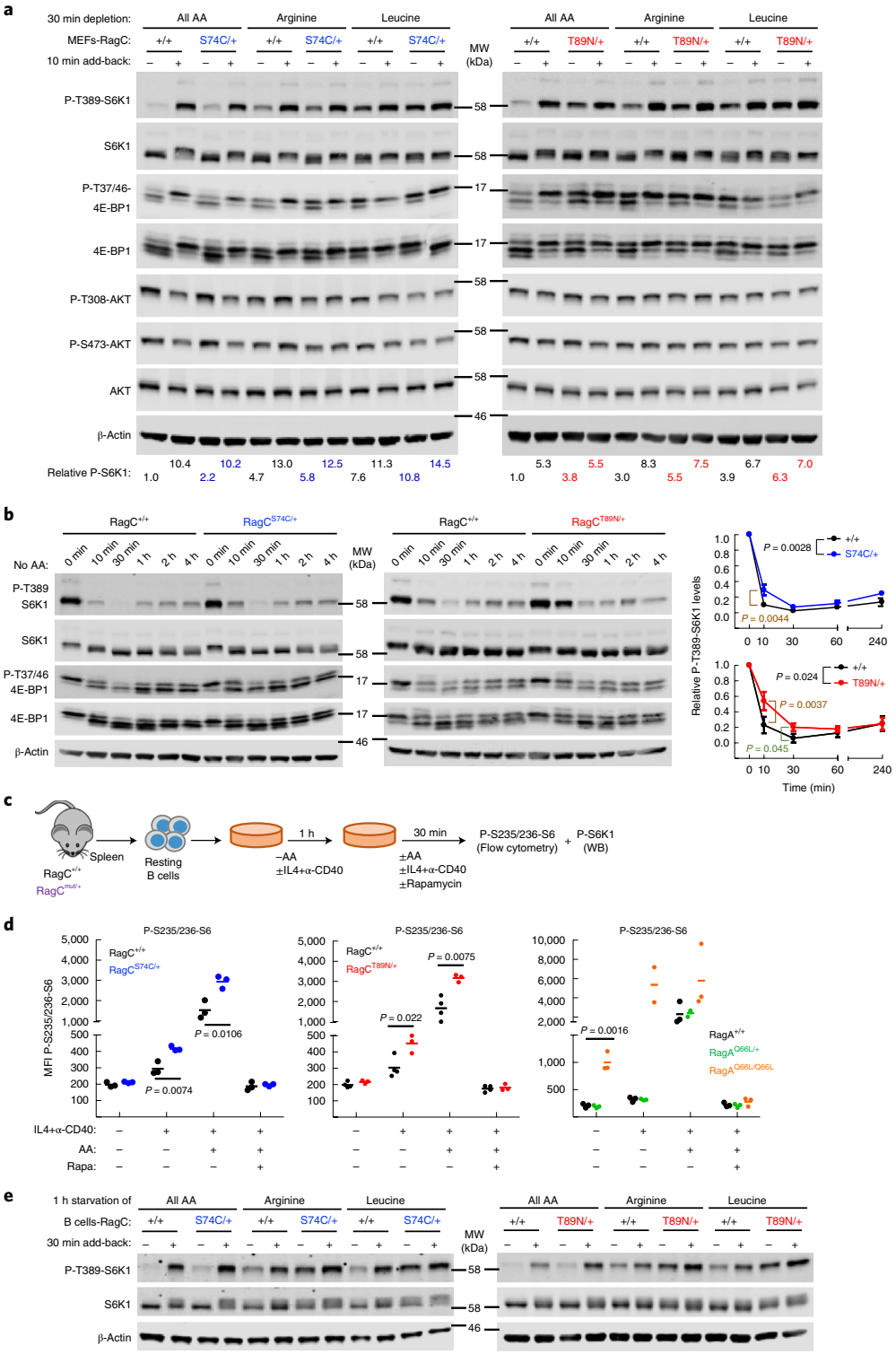

Fig. 1 | RagC mutant cells are partially resistant to amino acid withdrawal. a, Primary E13.5 MEFs of RagC$^{+/+}$, RagC$^{S74C/+}$ and RagC$^{T89N/+}$ genotypes were deprived of all amino acids (AA), arginine or leucine in RPMI supplemented with dialysed FBS for 30 min and re-stimulated for 10 min. Whole-cell protein lysates were immunoblotted for the indicated proteins. Quantification of P-S6K1 relative to the levels in RagC$^{+/+}$ cells without amino acids is shown. **b**, Same as **a**, but MEFs were deprived of all amino acids for the indicated times. Quantification of P-S6K1 is shown for $n=3$ independent MEFs per genotype. A statistically significant increase in mTORC1 signalling was found for 10 and 30 min in RagC$^{T89N/+}$ MEFs and for 10 min in RagC$^{S74C/+}$ MEFs. The *P* values next to the genotypes state the statistical significance of the analysis of area under the curve calculated during the first 30 min of starvation. Error bars indicate standard deviation. Statistical significance was calculated by two-tailed Student´s *t*-test. **c**, Experimental set-up for purification and acute in vitro stimulation of B cells. CD43^{-} naïve B cells were collected from spleens of indicated genotypes and stimulated in culture with anti (α)-CD40 and IL-4 in the presence or absence of all amino acids. WB, western blot. **d**, mTORC1 activity revealed by intracellular phospho-S6 staining after stimulation and quantification by flow cytometry of the indicated RagC and RagA genotypes. ($n=3$ for RagC$^{+/+}$, RagC^{S74C} and RagC$^{T89N/+}$; RagA$^{+/+}$ and RagA$^{Q66L/+}$; $n=2$ for RagA$^{Q66L/Q66L}$). **e**, Primary B cells were treated as in **d** and whole-cell protein lysates were immunoblotted for the indicated proteins.

autoimmunity-free) was significantly shorter in VavP-Bcl2^{tg}; RagC^{mut} (RagC$^{S74C/+}$ and RagC$^{T89N/+}$) mice (Fig. 2a and Supplementary Fig. 2g). These results suggest that deregulation of the nutrient sensing pathway deeply affects B cell functions to promote not only FL but also other pathological outcomes of aberrant B cell activation, such as autoimmune disease.

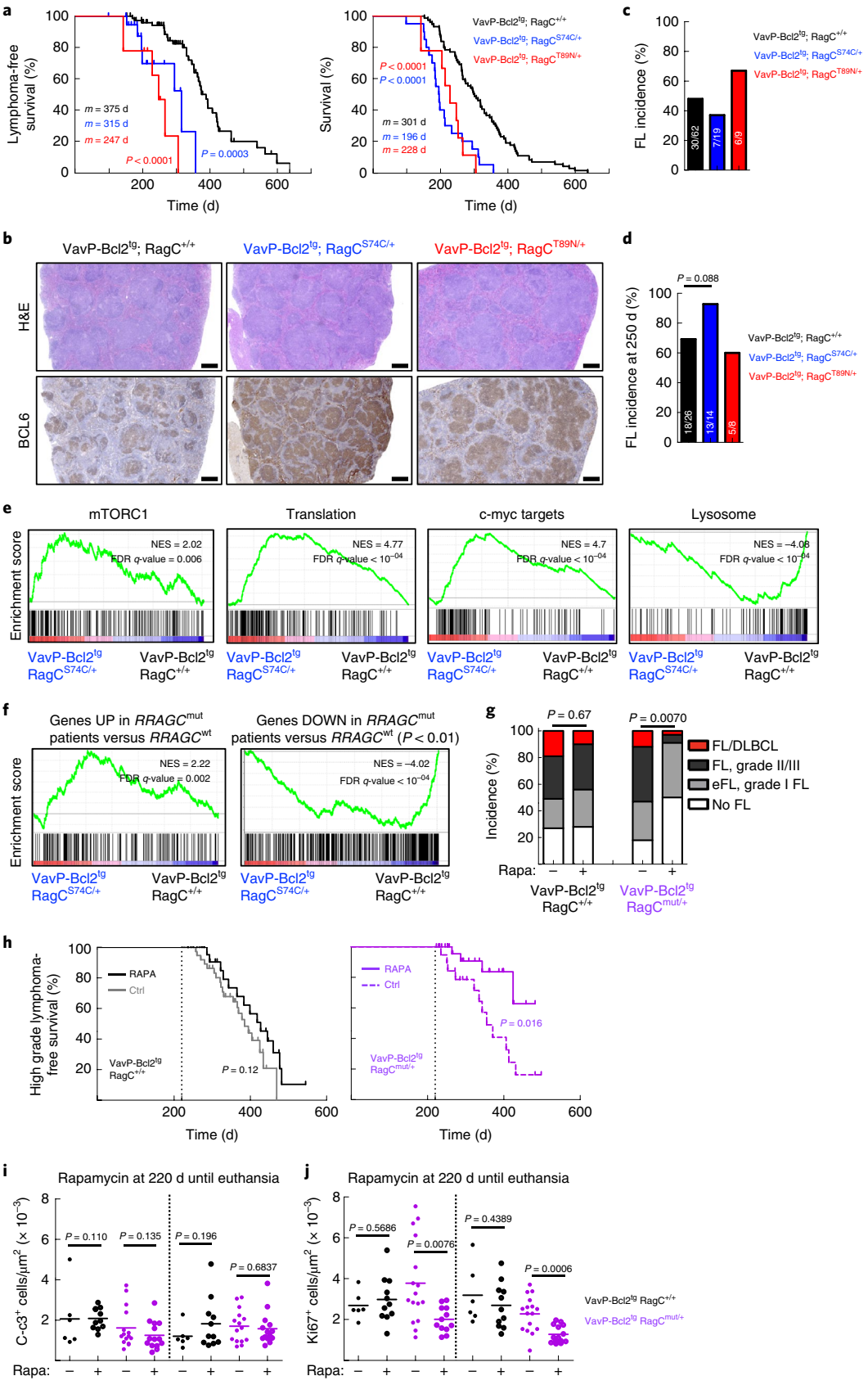

Considering that the expression of the mutations is neither conditional nor restricted to B cells, the striking similarities of latencies and diagnoses of RagC^{mut} mice and RagC^{mut} BM chimeras support a negligible impact of systemic expression of the mutations in B cell biology and lymphomagenesis.

To investigate the mechanisms underlying the oncogenicity of RagC^{mut}, we sorted B220^{+} cells from VavP-Bcl2^{tg}; RagC^{mut} and RagC^{wt} FLs and performed transcriptional profiling analysis. The agnostic gene-set enrichment analysis (GSEA)[35] showed the expected mTORC1 signalling signature enrichment in RagC mutant FL cells, together with other signatures consistent with mTORC1 activation, such as translation, c-myc targets and suppression of lysosomal biogenesis (Fig. 2e, see details of the signatures in Supplementary Table 1). We next performed a side-by-side comparison of transcriptional profiles obtained from murine and human FL samples of RagC^{wt} and RagC^{mut} genotypes[20] and observed that mRNAs selectively upregulated in murine RagC mutant FL samples were consistently enriched in *RRAGC* mutant human FL (and vice versa for downregulated genes (Fig. 2f), supporting the translational relevance of analysing RagC mutant mice for understanding human FL.

We reasoned that the mTOR inhibitor rapamycin would be particularly efficacious against FL arising in RagC mutant mice, and we administered rapamycin orally starting at 220 days to a cohort of VavP-Bcl2^{tg}; RagC^{mut} and VavP-Bcl2^{tg}; RagC^{wt} mice and monitored their survival thereafter. Rapamycin treatment strongly suppressed the phosphorylation of S240/244 of S6, a readout of mTORC1 signalling, in all lymphomas (Supplementary Fig. 2h). Importantly, the incidence and grade of lymphomas were lower in the rapamycin-treated RagC^{mut} mice, compared with untreated controls (Fig. 2g), with no statistical change in the incidence or the grade of lymphomas arising in RagC^{wt} mice. Pharmacological inhibition of mTORC1 did not extend the survival of mice with lymphomas of all grades (Supplementary Fig. 2i), but, interestingly, when we limited the analysis of lymphoma-free survival to mice with lymphomas of higher grade (grade II/III FL and FL/diffuse large B cell lymphoma (DLBCL), Fig. 2g), rapamycin selectively extended the survival of VavP-Bcl2^{tg}; RagC^{mut} mice, but not that of VavP-Bcl2^{tg}; RagC^{wt} mice (Fig. 2h). A short oral rapamycin treatment (for 7 days starting at 220 days) induced acute shrinking of spleens and a strong cell-cycle arrest, as measured by Ki67 staining, both in VavP-Bcl2^{tg}; RagC^{wt} and VavP-Bcl2^{tg}; RagC^{mut} mice (Supplementary Fig. 2j,k). Importantly, and supporting a selective antitumoral effect of rapamycin for RagC^{mut} mice, only the spleens of treated RagC^{mut} mice were significantly smaller after long-term rapamycin treatment (Supplementary Fig. 2j). Finally, and without a detectable pro-apoptotic effect (Fig. 2i), long-term rapamycin treatment inhibited proliferation selectively in RagC^{mut} FL (Fig. 2j), a selectivity also seen in the quantification of tumour burden (Supplementary Fig. 2l). Altogether, these data strongly support a selective long-term sensitivity to mTORC1 inhibition in tumours with activating mutations in the nutrient signalling pathway, and this sensitivity may be more profound in FL of higher grade.

As a whole, the results in Fig. 2 provide bona fide support for a critical oncogenic role for the *RRAGC* mutations in human FL. Moreover, our results show features of selective sensitivity of *Rragc* mutant FL to pharmacological inhibition of mTORC1 in vivo. Hence, our data nominate mutations in the nutrient signalling pathway as potential markers for patients who would benefit from treatment with mTOR inhibitors.

B cell functions are exacerbated in RagC mutant mice. To determine whether RagC mutations would drive aberrant B cell function in the context of physiological humoral responses, we analysed the primary response of RagC mutant B cells to intraperitoneal immunization with sheep red blood cells (SRBC) to induce GC formation (Supplementary Fig. 3a). We observed an approximately threefold increase in abundance of GC B cells in the spleens of RagC$^{S74C/+}$ and RagC$^{T89N/+}$ mice compared with RagC$^{+/+}$ mice at 10 days after immunization, close to the peak of the GC reaction (Fig. 3a). Histological analysis and immunohistochemical staining of spleen sections for the GC marker Bcl6 showed that GCs were both larger and more abundant in RagC mutant mice (Fig. 3a and Supplementary Fig. 3b). In contrast, activating mutations in RagA, which is not mutated in human FL, either in heterozygosity or in homozygosity, led to no measurable GC enlargement under similar conditions (Supplementary Fig. 3c), indicating an exquisite sensitivity of B cells to different degrees of activation of the nutrient signalling pathway. GC formation leads eventually to differentiation of GC B cells into antibody-secreting plasma cells (PCs). Accordingly, RagC mutant mice showed an approximately threefold increase in the abundance of splenic PCs (Fig. 3b). Consistent with increased PC production in RagC$^{S74C/+}$ and RagC$^{T89N/+}$ mice, the titre of class-switched, IgG1 antibodies in serum quantified 10 days after immunization was markedly increased compared with that of RagC$^{+/+}$ mice (Fig. 3c). The exacerbated humoral response to SRBC in RagC mutant mice was sensitive to rapamycin treatment, when administered for the entire humoral response period assessed (10 days) and when restricted to the last 2 days, after GC entry (Supplementary Fig. 3d). Collectively, these results show that RagC mutations enhance the humoral response to SRBC, but do not block differentiation of GC B cells to PCs.

Fig. 2 | Accelerated lymphomagenesis by heterozygous expression of mutant RagC in mice with selective sensitivity to rapamycin. a, Kaplan–Meier lymphoma-free survival (left) and survival (right) curves of VavP-Bcl2^{tg}; RagC$^{+/+}$ ($n=74$), VavP-Bcl2^{tg}; RagC$^{S74C/+}$ ($n=20$) and VavP-Bcl2^{tg}; RagC$^{T89N/+}$ ($n=9$) mice. In lymphoma-free survival curves, mice that developed FL were scored as 1. Statistical significance was calculated with the log-rank test; *m*: median survival. **b**, Representative H&E and anti-Bcl6 IHC from spleen sections from FL-bearing mice (more than 90 tumours analysed). Scale bar, 500 µm. **c**, Incidence of FL in cohorts shown in **a**. **d**, Incidence of FL in cohorts euthanized at 250 d. Statistical significance was calculated by chi-squared test. **e**, Enrichment of gene signatures (GSEA) related to mTORC1 signalling, genes involved in translation, c-myc targets and lysosomal genes in VavP-Bcl2^{tg}; RagC$^{S74C/+}$ FL sorted cells ($n=4$ mice) compared to VavP-Bcl2^{tg}; RagC$^{+/+}$ FL sorted cells ($n=7$ mice). **f**, GSEA in VavP-Bcl2^{tg}; RagC$^{S74C/+}$ compared to VavP-Bcl2^{tg}; RagC$^{+/+}$ FL sorted cells, on the list of significantly upregulated and downregulated genes in *RRAGC* mutant human FL samples. NES: normalized enrichment score; FDR: false discovery rate. **g**, Incidence and histological grades of tumours in mice treated with rapamycin and controls. (All mice were VavP-Bcl2^{tg}: RagC$^{+/+}$ – Rapa $n=41$, RagC$^{+/+}$ + Rapa $n=32$; RagC^{mut} – Rapa $n=17$; RagC^{mut} + Rapa $n=32$.) Mice that developed tumours before 220 d were excluded. Statistical significance was calculated with chi-squared test. **h**, Kaplan–Meier lymphoma-free survival curves (FL-grade II, FL-grade III and diffused tumours were scored as 1, mice bearing no FL, early FL and FL-grade I scored as 0) of mice untreated or treated with rapamycin starting at 220 d (vertical dotted line). All mice were VavP-Bcl2^{tg}: RagC$^{+/+}$ – Rapa $n=43$, RagC$^{+/+}$ + Rapa $n=32$; RagC^{mut} – Rapa $n=19$; RagC^{mut} + Rapa $n=34$). Statistical significance was calculated with the log-rank test. **i**, Quantification of C-c3 in spleens and lymph nodes (LN) from rapamycin (Rapa)-treated ($n=11$ VavP-Bcl2^{tg}; RagC$^{+/+}$ and $n=14$ VavP-Bcl2^{tg}; RagC^{mut}) and untreated mice ($n=6$ VavP-Bcl2^{tg}; RagC$^{+/+}$ and $n=15$ VavP-Bcl2^{tg}; RagC^{mut}). **j**, Quantification of Ki67 in VavP-Bcl2^{tg}; RagC$^{+/+}$ and VavP-Bcl2^{tg}; RagC^{mut} in spleens and LN from Rapa-treated ($n=11$ VavP-Bcl2^{tg}; RagC$^{+/+}$ and $n=14$ VavP-Bcl2^{tg}; RagC^{mut}) and untreated mice ($n=6$ VavP-Bcl2^{tg}; RagC$^{+/+}$ and $n=15$ VavP-Bcl2^{tg}; RagC^{mut}). In **i** and **j** statistical significance was calculated by two-tailed Student's *t*-test and lines indicate mean.

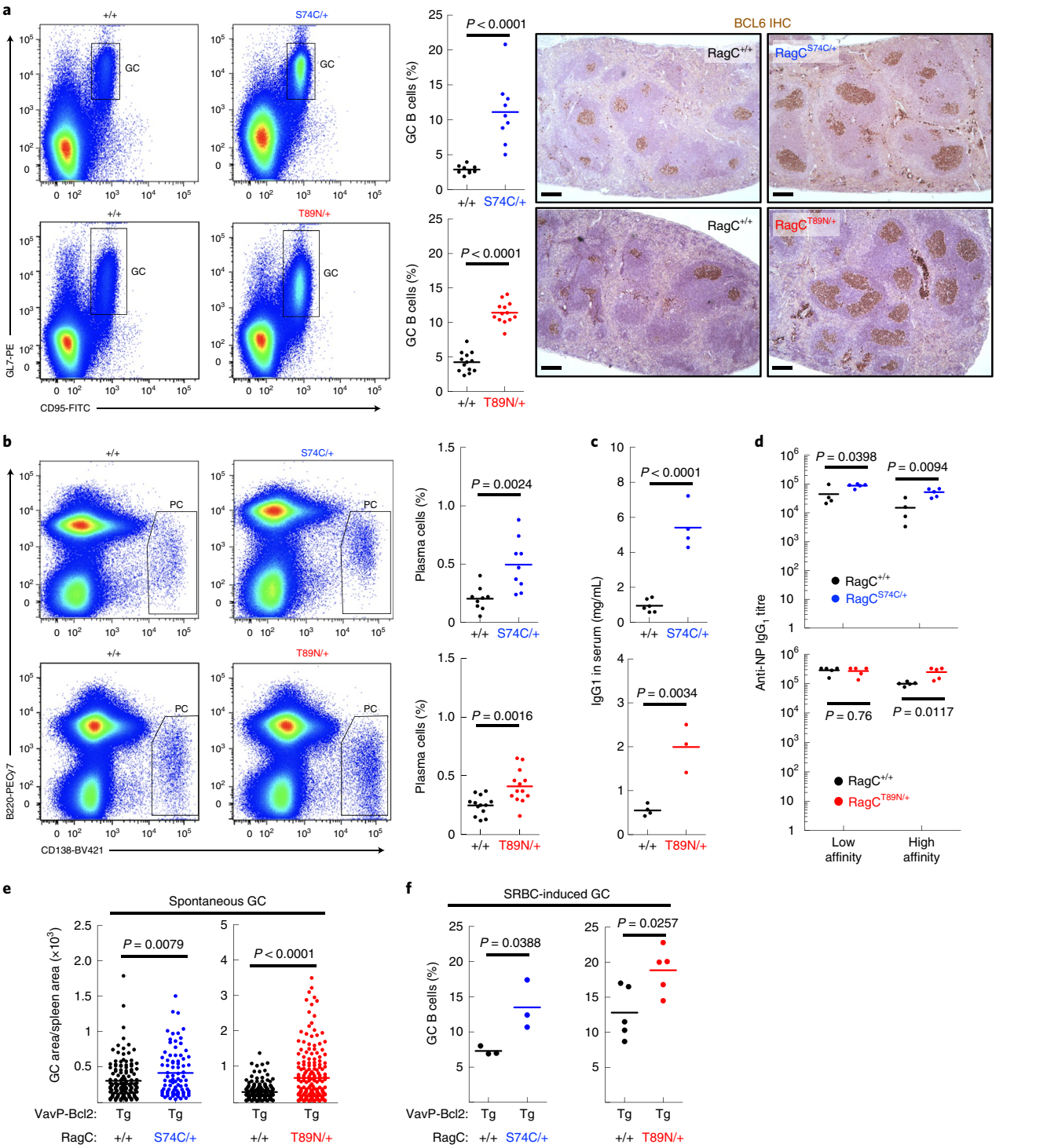

Fig. 3 | Exacerbated humoral response in RagC mutant mice. a, Representative flow cytometry plots (B220$^+$ gated, GL7$^+$ and CD95$^+$), quantification and IHC staining anti-Bcl6, in spleens collected from RagC$^{+/+}$ ($n=9$) and RagC$^{S74C/+}$ ($n=9$), RagC$^{+/+}$ ($n=13$) and RagC$^{T89N/+}$ ($n=13$) chimeras 10 d after immunization with SRBC. Scale bar, 100 µm. **b**, Representative flow cytometry plots (B220^{low} and CD138$^+$) and quantification of PCs in spleens from RagC$^{+/+}$ ($n=9$) and RagC$^{S74C/+}$ ($n=9$), RagC$^{+/+}$ ($n=13$) RagC$^{T89N/+}$ ($n=13$) chimeras 10 d after immunization with SRBC. **c**, IgG1 quantification from sera from RagC$^{+/+}$ ($n=6$ and $n=4$), RagC$^{S74C/+}$ ($n=4$) and RagC$^{T89N/+}$ ($n=3$) chimeras 10 d after immunization with SRBC, measured by ELISA. **d**, Anti-NP-IgG1 low- and high-affinity serum titres were determined by ELISA in RagC$^{+/+}$ ($n=4$ and $n=5$), RagC$^{S74C/+}$ ($n=5$) and RagC$^{T89N/+}$ ($n=5$) chimeras. Serum was collected 28 d after NP-KLH immunization. **e**, Quantification of spontaneous GC formation, as determined by Bcl6 IHC, from the spleen sections of young VavP-Bcl2^{tg}; RagC$^{S74C/+}$ mice ($n=133$ GCs analysed from three VavP-Bcl2^{tg}; RagC$^{+/+}$ mice and 83 GCs analysed from three VavP-Bcl2^{tg} RagC$^{S74C/+}$ mice; 6–13 weeks old) and VavP-Bcl2^{tg}; RagC$^{T89N/+}$ mice ($n=169$ GCs analysed from five VavP-Bcl2^{tg}; RagC$^{+/+}$ mice, $n=193$ GCs analysed from six VavP-Bcl2^{tg}; RagC$^{T89N/+}$ mice, 6–11 weeks old). Dots represent Bcl6 area of each GC normalized by total area of the spleen section. **f**, Quantification of GC B cells (B220$^+$ gated, GL7$^+$ and CD95$^+$) in spleens collected from VavP-Bcl2^{tg}; RagC$^{S74C/+}$ and VavP-Bcl2^{tg}; RagC$^{T89N/+}$ chimeras 10 d after immunization with SRBC ($n=3$ VavP-Bcl2^{tg}; RagC$^{+/+}$, $n=3$ VavP-Bcl2^{tg}; RagC$^{S74C/+}$, $n=5$ VavP-Bcl2^{tg}; RagC$^{+/+}$ and $n=5$ VavP-Bcl2^{tg}; RagC^{T89N}). In all panels, horizontal lines indicate the mean; statistical significance was calculated by two-tailed Student's *t*-test.

Constitutive activation of the mTORC1 pathway by expression of RagA^{GTP} or by deletion of Tsc1 in B cells is detrimental to affinity maturation[36] and outcome of the GC reaction, together with the production of memory B cells. This impairment occurs presumably because constitutive mTORC1 activity in all GC B cells, instead of its selective dynamic increase in cells with comparatively higher affinity antibodies, precludes affinity-based positive selection[36]. To determine whether affinity maturation was also impaired in

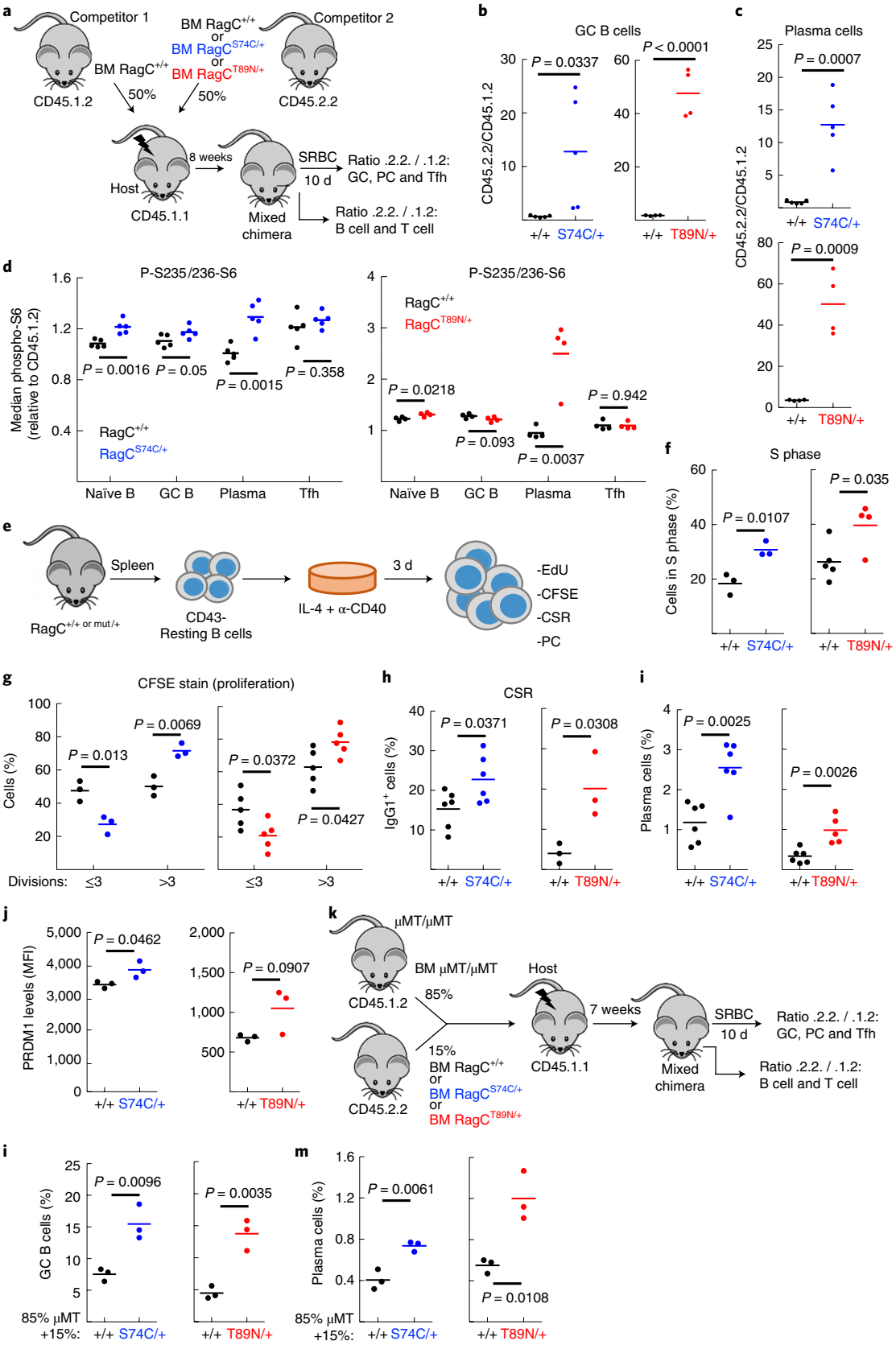

mice with mutations in RagC, we immunized mice intraperitoneally with the hapten-carrier complex 4-hydroxy-3-nitrophenylacetyl-keyhole limpet haemocyanin (NP-KLH) in alum, and quantified the increase in high-affinity NP antibodies in serum over a 28-day period by affinity-dependent enzyme-linked immunosorbent assay (ELISA) (Supplementary Fig. 3e). Surprisingly, and in contrast to decreased high-affinity titre of antibodies of $RagA^{GTP}$ and Tsc1 knockout models of deregulated mTORC1 activity[36], $RagC^{S74C/+}$ and $RagC^{T89N/+}$ mice showed increased production of high-affinity antibodies to NP (Fig. 3d).

Next, we determined whether exacerbated B cell functions were also at work in mice expressing RagC mutations in the context of overexpression of BCL2, but before the onset of FL. We first quantified spontaneous GC formation in unimmunized mice, readily observed in VavP-$Bcl2^{tg}$; $RagC^{wt}$ controls[34], and observed a significant expansion of GC area in VavP-$Bcl2^{tg}$; $RagC^{mut}$ (Fig. 3e). Moreover, 10 days after SRBC immunization we observed a similar approximately two- to threefold expansion in GC B cells in VavP-$Bcl2^{tg}$; $RagC^{mut}$ (Fig. 3f). These results indicate that exacerbated B cell activation caused by endogenous expression of RagC mutations also occurs in the cellular context of Bcl2 overexpression, which will result in follicular lymphomagenesis.

Altogether, the results obtained with SRBC and NP-KLH immunizations show that RagC mutant mice have an exacerbated humoral response, with increased GC size and cellularity and PC production, but without impaired selection of high-affinity B cells or compromised production of high-affinity antibodies. Hence, a mild, partial gain-of-function in the nutrient signalling arm of mTORC1 favours expansion of activated B cells, even in the context of Bcl2 overexpression. This aberrant behaviour is consistent with the oncogenic potential of RagC mutations, and contrasts to the cell-intrinsic deleterious effects of more profound perturbations in mTORC1 activity as elicited by $RagA^{GTP}$ or loss of Tsc1 (ref. [36]).

Enhanced B cell activation in RagC mutants is cell intrinsic. To ascertain whether RagC mutant cells had a competitive advantage relative to RagC wild-type cells, as suggested by the results of immunization (Fig. 3), we performed competitive reconstitution in lethally irradiated hosts by co-injecting $RagC^{+/+}$ and either $RagC^{S74C/+}$ or $RagC^{T89N/+}$ BM cells in a 1:1 ratio, traceable by the differential expression of CD45.1 and CD45.2 (Fig. 4a). The behaviour and abundance of RagC mutant cells during competitive haematopoiesis, B cell lineage development and immunization and GC formation were then monitored. We first determined the contribution to lymphoid populations (mature B and T lymphocytes) in the spleen 2 months after reconstitution by cell surface immunostaining of the alleles CD45.1 and CD45.2. We observed that cells of the RagC mutant genotype marginally but significantly outnumbered wild-type cells in the $B220^+$ naïve B cell compartment (Supplementary Fig. 4a), while showing no competitive advantage in generating T cells (Supplementary Fig. 4a). More importantly, when we immunized the mixed chimeras with SRBC, we observed a greater enrichment of RagC mutant cells in the GC B cell population (~18-fold for $RagC^{S74C/+}$; and ~27-fold for $RagC^{T89N/+}$). A similar enrichment was found in the PC population (~14-fold for $RagC^{S74C/+}$; ~14-fold for $RagC^{T89N/+}$) (Fig. 4b,c and Supplementary Fig. 4b,c). Monitoring of mTORC1 activity in different B cell populations (naïve, GC and PC) showed increased phospho-S6 in $RagC^{mut}$ cells compared with $RagC^{wt}$ cells cohabiting the same spleen (Fig. 4d). In contrast to the competitive advantage of B cells, RagC mutant GC-resident T lymphocytes (follicular helper T cells, Tfh) were only marginally, and not significantly, enriched over wild-type competitors (Supplementary Fig. 4d), with no significant differences in mTORC1 activity (Fig. 4d). Together, our results show that RagC mutations confer a modest but significant increase in mTORC1 activity in B cell populations, which is associated with increased competitiveness of mutant B cells during B cell lineage development, and, markedly, during the GC response. The increased fitness of RagC mutant GC B cells is prone to playing a role in enriching the population of RagC mutant cells during the multiple cellular competition events occurring during the protracted course of the development of FL.

In contrast to the strong effects on B cells, RagC mutations had minimal impact on T cell development or Tfh differentiation, suggesting that B cell phenotypes are strongly cell autonomous. In addition, these results suggested that RagC mutant B cells may be less dependent on T cell help for activation. To test this, we mimicked T cell help to B cells in vitro by incubation with anti-CD40 (Fig. 4e). This treatment elicited several features of enhanced dose-dependent activation of RagC mutant B cells, such as increased proliferation, measured by EdU incorporation and by carboxyfluorescein succinimidyl ester (CFSE) label decay, increased class-switch recombination to IgG1 and increased PC differentiation, as measured by expression of PC surface marker CD138 and intracellular *Prdm1* (Fig. 4f–j and Supplementary Fig. 4e–i). As seen in vivo (Supplementary Fig. 3d) and as expected, in vitro activation of

Fig. 4 | B cell-intrinsic activation and increased fitness by expression of RagC mutations. a, Experimental set-up of in vivo B lymphocyte competition experiments with mixed BM chimeras. BM reconstitution of lethally irradiated CD45.1.1 hosts, by co-injecting $RagC^{+/+}$ (CD45.1.2) and either $RagC^{+/+}$, $RagC^{S74C/+}$ or $RagC^{T89N/+}$ (CD45.2.2) BM cells in a 1:1 ratio. After 8 weeks, reconstituted mice were immunized with SRBC. **b**, Quantification of CD45.2.2/CD45.1.2 ratio in GC B cells ($B220^+CD95^+GL7^+$gated) in splenocytes collected from mixed chimeras 10 d after immunization ($n=5$ for $RagC^{+/+}-RagC^{+/+}$ and $n=5$ for $RagC^{+/+}-RagC^{S74C/+}$; $n=5$ for $RagC^{+/+}-RagC^{+/+}$ and $n=4$ for $RagC^{+/+}-RagC^{T89N/+}$). **c**, Quantification of CD45.2.2/CD45.1.2 ratio in PCs ($B220^{low}CD138^+$ gated) in splenocytes collected from mixed chimeras 10 d after immunization (n for each genotype as in **b**). **d**, Quantification of S235/236-phosphorylation of S6 in naïve ($B220^+CD95^-GL7^-$), GC B ($B220^+CD95^+GL7^+$), PC ($B220^{low}CD138^+$) and Tfh ($CD4^+CXCR5^+PD1^+$) populations from spleens collected from mixed chimeras 10 d after immunization ($n=5$ for $RagC^{+/+}-RagC^{+/+}$ and $n=5$ for $RagC^{+/+}-RagC^{S74C/+}$; $n=4$ for $RagC^{+/+}-RagC^{+/+}$ and $n=4$ for $RagC^{+/+}-RagC^{T89N/+}$). **e**, Experimental set-up of in vitro B cell activation. Naïve B cells were isolated from spleens of $RagC^{+/+}$, $RagC^{S74C/+}$ and $RagC^{T89N/+}$ mice by using CD43 magnetic beads. $CD43^-$ cells were stimulated with anti-CD40 and IL-4. Three days after activation, the following parameters (**f**–**j**) were quantified. **f**, S phase determined by EdU incorporation in $CD19^+$ cells ($n=3$ for $RagC^{+/+}$ and $RagC^{S74C/+}$; $n=5$ for $RagC^{+/+}$ and $n=4$ for $RagC^{T89N/+}$). **g**, Proliferation by CFSE staining in $B220^+$ cells ($n=3$ for $RagC^{+/+}$ and $RagC^{S74C/+}$; $n=5$ for $RagC^{+/+}$ and $RagC^{T89N/+}$). **h**, Quantification of class-switched $B220^+IgG1^+$ cells ($n=6$ for $RagC^{+/+}$ and $RagC^{S74C/+}$; $n=3$ for $RagC^{+/+}$ and $RagC^{T89N/+}$). CSR, class-switch recombination. **i**, PC production by expression of cell surface marker CD138 in $B220^{low}$ cells ($n=6$ for $RagC^{+/+}$ and $RagC^{S74C/+}$; $n=6$ for $RagC^{+/+}$ and $n=5$ for $RagC^{T89N/+}$). **j**, PC production by intracellular immunostaining of PRDM1 in $B220^{low}$ $CD138^+$ cells quantified by flow cytometry. $n=3$ mice per genotype. MFI: median fluorescence intensity. **k**, Experimental set-up for determining cell-intrinsic effects of RagC mutations using mixed BM chimeras with the $Ighm^{\mu MT}$ genetic system[37]. BM reconstitution of lethally irradiated CD45.1.1 hosts, by co-injecting $Ighm^{\mu MT/\mu MT}$ (CD45.1.2) and either $RagC^{+/+}$, $RagC^{S74C/+}$ or $RagC^{T89N/+}$ (CD45.2.2) BM cells in a 9:1 ratio. After 8 weeks, mice were immunized with SRBC. Quantification of GC B cells ($B220^+CD95^+GL7^+$) (**l**) and PC ($B220^{low}CD138^+$) (**m**), in spleens collected from $Ighm^{\mu MT/\mu MT}$: $RagC^{+/+}$, $RagC^{S74C/+}$ or $RagC^{T89N/+}$ 10 d after immunization ($n=3$ mice per genotype). In all panels, lines indicate the mean and statistical significance was calculated by two-tailed Student's t-test.

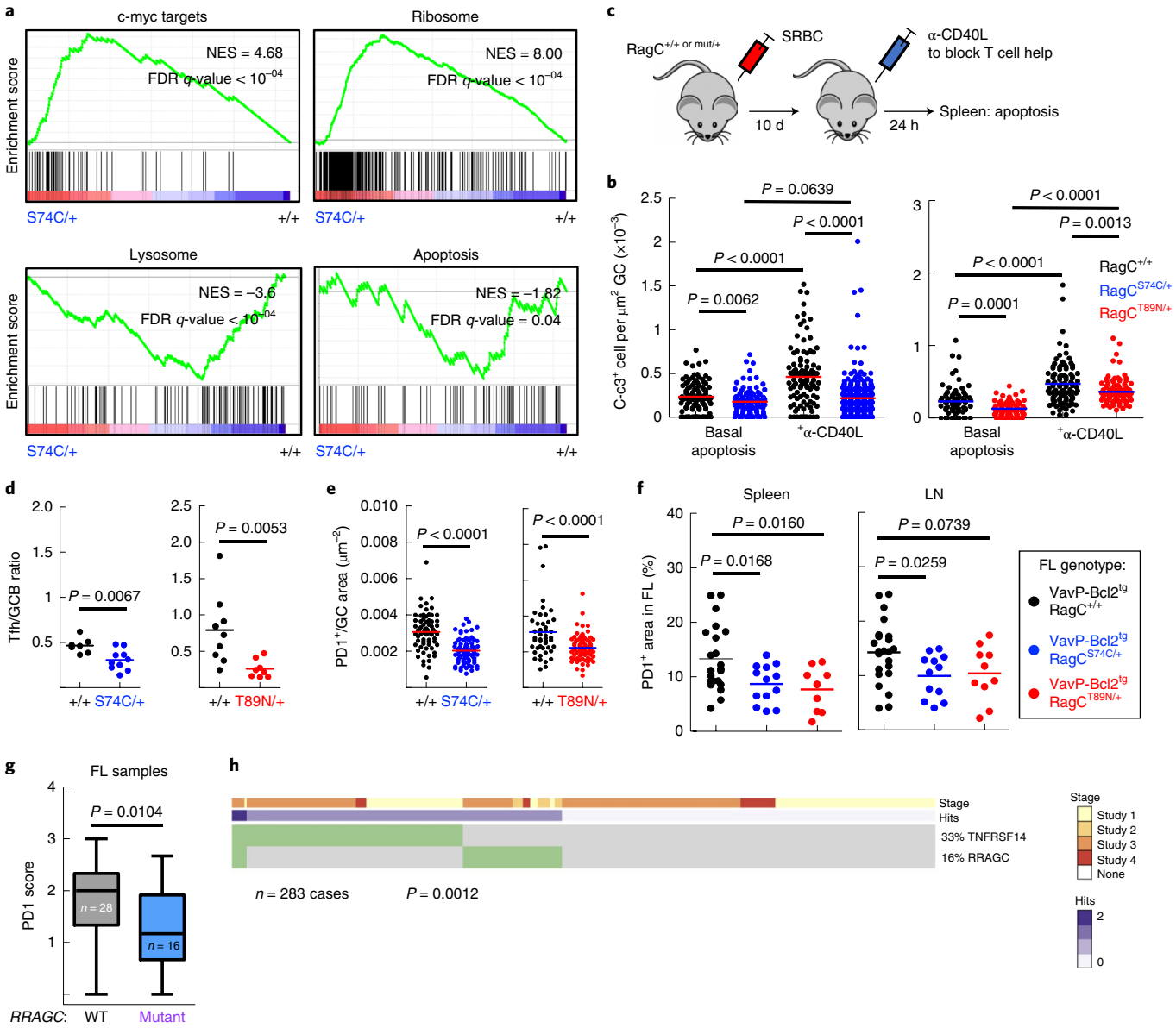

Fig. 5 | Impact of RagC mutations in Tfh-mediated B cell activation and apoptosis in FL. a, Enrichment of gene signatures related to c-myc targets and ribosomal genes in RagC$^{S74C/+}$ ($n=4$ mice) versus RagC$^{+/+}$ GC B cells ($n=4$ mice); and enrichment of gene signatures related to lysosomal genes and apoptotic genes in RagC$^{+/+}$ versus RagC$^{S74C/+}$ GC B cells. **b**, Quantification of C-c3$^+$ cells within the GC area (Bcl6$^+$ cells) in RagC$^{+/+}$, RagC$^{S74C/+}$ and RagC$^{T89N/+}$ mice 10 d after immunization with SRBC and following a 24-h injection of 200 µg of anti-CD40L. Dots represent C-c3$^+$ cells per GC area (basal apoptosis: $n=101$ GCs analysed in five RagC$^{+/+}$ mice, $n=118$ GCs from five RagC$^{S74C/+}$ mice, $n=77$ GCs from five RagC$^{+/+}$ mice, $n=80$ GCs analysed in five RagC$^{T89N/+}$ mice, anti-CD40L-induced apoptosis: $n=105$ GCs from three RagC$^{+/+}$ mice, $n=273$ GCs from four RagC$^{S74C/+}$ mice; $n=102$ GCs from four RagC$^{+/+}$ mice, $n=105$ GCs from four RagC$^{T89N/+}$ mice). **c**, Experimental set-up for induction of apoptosis by blocking Tfh-mediated B cell activation in mice immunized with SRBC. **d**, Quantification of Tfh/GC B cell ratio in spleens collected from RagC$^{+/+}$, RagC$^{S74C/+}$ and RagC$^{T89N/+}$. Percentage of GC B cells was calculated from CD19$^+$CD95$^+$CD38$^-$ cells. Percentage of Tfh cells was calculated from CD4$^+$CXCR5$^+$PD1$^+$ cells ($n=7$ RagC$^{+/+}$, $n=10$ RagC$^{S74C/+}$, $n=10$ RagC$^{+/+}$, $n=8$ RagC$^{T89N/+}$. **e**, Quantification of PD1$^+$ cells within the GC area in RagC$^{+/+,\ S74C/+\ and\ T89N/+}$ mice 10 d after immunization with SRBC ($n=67$ GCs from three RagC$^{+/+}$ mice and $n=87$ GCs from three RagC$^{S74C/+}$ mice; $n=47$ GCs from three RagC$^{+/+}$ mice and $n=70$ GCs from four RagC$^{T89N/+}$ mice). **f**, Quantification of PD1$^+$ area in RagC$^{+/+}$ ($n=22$), RagC$^{S74C/+}$ ($n=13$) and RagC$^{T89N/+}$ ($n=9$) (all VavP-Bcl2^{tg}) mice, in spleen and LN areas affected by FL. Lines indicate the mean (**b**,**d**–**f**); statistical significance was calculated by two-tailed Student's *t*-test. **g**, Quantification of PD1$^+$ cells in untreated human FL samples relative to *RRAGC* mutational status. The box-whiskers plot indicate the mean (horizontal line), 25–75% range (box) and whiskers indicate maximum and minimum values. Statistical significance was calculated with one-tailed Mann–Whitney *U*-test. **h**, Oncoprint of 283 cases with *TNFRSF14* and *RRAGC* mutations showing a mutually exclusive pattern. Study 1 (ref. [40]): 109 cases, Study 2 (ref. [19]): 12 cases; Study 3 (ref. [20]): 141 cases, Study 4 (ref. [17]): 21 cases. Total: 283 cases. Statistical significance was calculated with one-sided Fisher's exact test.

B cells and PC differentiation were sensitive to acute rapamycin treatment (Supplementary Fig. 4j).

To confirm the B cell-intrinsic causality of exacerbated B cell activation by RagC mutations in vivo, we undertook a genetic approach consisting of BM reconstitution with a majority (85–90%) of Ighm$^{\mu MT/\mu MT}$ haematopoietic stem cells (HSCs), which are unable to produce a B cell lineage[37], mixed with 10–15% of RagC$^{+/+}$, RagC$^{S74C/+}$ or RagC$^{T89N/+}$ HSC (Fig. 4k). In this setting, T lymphocytes and

all myeloid cells derive almost exclusively from (RagC wild-type) Ighm$^{\mu MT/\mu MT}$ HSCs, but the B cell lineage descends entirely from RagC mutant (or wild-type in control mice) progenitors (Supplementary Fig. 4k). When these mixed BM chimeras were immunized with SRBC as before, we observed that expression of RagC^{S74C} or RagC^{T89N} mutations restricted to B cells sufficed to drive the same enhancement in GC formation and size (Fig. 4l) and PC generation (Fig. 4m) as observed in single-population RagC mutant BM chimeras and in full-body RagC mutant mice. Hence, exacerbated B cell activation occurs by the expression of RagC mutants in a cell-intrinsic manner.

RagC mutants show decreased supportive T cell signals. To gain insight into the cellular events underlying the exacerbated B cell activation, we next compared the transcriptional profiles of sorted GC B cells from RagC wild-type and RagC mutant mice. The transcriptome of sorted GC cells arising from RagC mutant and wild-type mice showed a striking overlap with signatures identified in FL cells (Supplementary Fig. 5a). This overlap supports the idea that the analysis of the GC reaction is a meaningful mirror of cellular states and processes occurring in FL. Target gene signatures of c-myc, indicative of a state of enhanced B cell activation[38,39] and synergistic with mTORC1 activity in GC cells[36], were also observed in RagC mutant GC and FL samples (Figs. 5a, 2e and Supplementary Fig. 5b). Furthermore, GSEA analysis also showed upregulation of gene signatures related to the activation of mTORC1 in RagC mutant GC, including ribosome biogenesis genes, and genes downregulated in lysosomal biogenesis (Fig. 5a and Supplementary Fig. 5b) and downregulated in a human B cell lymphoma line (BJAB) treated with rapamycin or deprived of leucine[41] (Supplementary Fig. 5c).

GSEA also revealed a signature of suppressed apoptosis in the RagC mutant GCs (Fig. 5a and Supplementary Fig. 5b), a process not generally perceived as regulated by mTORC1 (refs. [42–45]). However, apoptosis has particular relevance in GC B cells, as programmed cell death is a frequent fail-safe response triggered on poor affinity or lack of T cell help, unresolved DNA damage or self-reactivity[2]. Indeed, the increased GC size and exacerbated B cell response were consistent with increased proliferation, suppressed apoptosis or both. Steady-state proliferation measured within the increased GC B cell population from RagC mutant mice was similar to that of wild-type mice (Supplementary Fig. 5d), suggesting that decreased death, rather than increased division, could partially explain the increase in the GC B cell population, and provide an explanation for the oncogenicity of RagC mutations. We validated the suppression of programmed cell death signature in RagC mutant GC B cells by immunostaining against cleaved caspase 3 (C-c3) 10 days after induction of GC by SRBC injection (Fig. 5b and Supplementary Fig. 5e). In an attempt to mechanistically connect decreased apoptosis in RagC mutant B cells to an indifference to T cell support, we induced a 'death-by-neglect' fate by injecting a blocking antibody to CD40 ligand (anti-CD40L), the key driver of Tfh help to GC B cells[36,46,47]. During the B-to-T synapse, ligation of the CD40 receptor in B cells activates several signalling cascades, including PI3K–Akt. Injection of anti-CD40L into mice previously immunized with SRBC (Fig. 5c) resulted in increased apoptosis, but significantly less so in RagC mutant versus wild-type chimeras, as determined by quantification of Bcl6/C-c3 double-positive GC B cells (Fig. 5b). Importantly, this reduction in apoptosis was not a reflection of a general resistance to cell death, as γ-irradiation with 5 Gy induced equally large amounts of Bcl6/C-c3 positive cells in wild-type and RagC mutant GC B cells (Supplementary Fig. 5f). This result indicates that RagC mutant GC B cells are intrinsically resistant to apoptosis on withdrawal of T cell help, and is consistent with a reduced need for microenvironmental activating Tfh signals in RagC mutant B cells. Indeed, while the overall abundance of Tfh gated on its parental CD4$^+$ population is not decreased in RagC mutant mice, the relative abundance of supportive Tfh cells in GC is markedly decreased because of the massive expansion of the GC, as evidenced by a higher ratio of GC B cells to Tfh cells determined by flow cytometry (Fig. 5d), and by lower Tfh abundance per GC area by immunostaining with the Tfh marker PD1 (Fig. 5e), again supporting that a relative reduction in follicular T help is well tolerated in RagC mutant B cells. We did not find evidence for transcriptional changes in RagC^{mut} GC cells in genes known to be involved in B-to-Tfh cross-talk in the GC synapse (Supplementary Table 2), supporting that B cells are less dependent on Tfh signals without paracrinally repelling Tfh or affecting their function[48–51].

Increased independence of GC B cells from Tfh cell signals conferred by RagC mutations may or may not be meaningful in the context of FL induced by VavP-Bcl2^{tg}, particularly if this independence is related to a suppression of apoptosis. To test this possibility, we first quantified steady-state apoptosis in GC induced on immunization in VavP-Bcl2^{tg}; RagC$^{wt\ or\ mut}$ mice. While apoptosis was suppressed by the expression of VavP-Bcl2, regardless of the RagC mutational status, we observed that VavP-Bcl2^{tg}; RagC^{mut} mice had significantly lower C-c3 compared with their VavP-Bcl2^{tg}; RagC^{wt} counterparts (Supplementary Fig. 5g). Next, we quantified Tfh cells in murine FL samples. RagC mutant FL showed a similar decrease in the abundance of Tfh cells by IHC (Fig. 5f) and by flow cytometry (CXCR5$^+$ PD1$^+$ Foxp3$^-$) (Supplementary Fig. 5h), again, without transcriptional changes in B-to-T signals (Supplementary Table 2).

We then analysed collections of untreated human FL biopsies harbouring mutations in *RRAGC*, and observed a similar decrease in the abundance of PD1-positive T cells in the follicular areas of these tumours (RagC^{wt}: 28 cases, RagC^{mut}: 16 cases; Fig. 5g and Supplementary Fig. 5i). The decrease in Tfh cell abundance was even stronger when samples harbouring co-occurring mutations in *RRAGC* and the lysosomal v-ATPase, both involved in the control of mTORC1 activation[52], were grouped (Supplementary Fig. 5j).

Finally, loss of *TNFRSF14* (HVEM) function (by genetic loss or mutation) is a frequent lesion in human FL because it induces a tumour-supportive microenvironment that includes increased Tfh cellularity[14]. If our hypothesis of RagC mutations conferring some degree of independence toward T cell help is true, then loss of *TNFRSF14* would be functionally redundant with mutations in *RRAGC*, and hence these two genetic events would be unlikely to be co-selected in the same patient sample. Hence, we performed a meta-analysis of all four reports of human FL samples for which information regarding the genomic mutational landscape, including the status of *RRAGC* and *TNFRSF14*, was available[17,19,20,40] and found that these two genetic lesions were mutually exclusive (Fig. 5h; $P=0.0012$). Because *TNFRSF14* can be inactivated by mutation or deletion, we performed an additional validation with a cohort of FL samples for which we obtained deletion plus mutation information for *TNFRSF14*, plus mutational data on *RRAGC*. In this cohort of 109 cases we validated the existence of mutual exclusivity between *RRAGC* mutations and *TNFRSF14* mutations or deletions (Fisher's exact test: $P=0.0367$; Supplementary Fig. 5k). Together, the lower abundance of Tfh cells from the tumour microenvironment and the mutually exclusive genetic alterations in *RRAGC* and *HVEM* suggest that FL may rely on alternative avenues to support its growth, by attracting Tfh cells by loss of *HVEM* or autonomously activating intracellular pathways that synergize with, and thus decrease its need for, Tfh cell-derived signals by mutations in *RRAGC* (Fig. 6).

Discussion

Using genetically engineered mice, we provide bona fide evidence for an oncogenic role of the Rag GTPase pathway. The exclusiveness of recurrent mutations in *RRAGC* in human B cell lymphomas (FL, and a smaller percentage of DLBCL) suggests that B lymphocytes are exquisitely sensitive to perturbations in the nutrient sensing pathway. Our previous work in mice with genetic deletion[53] and constitutive

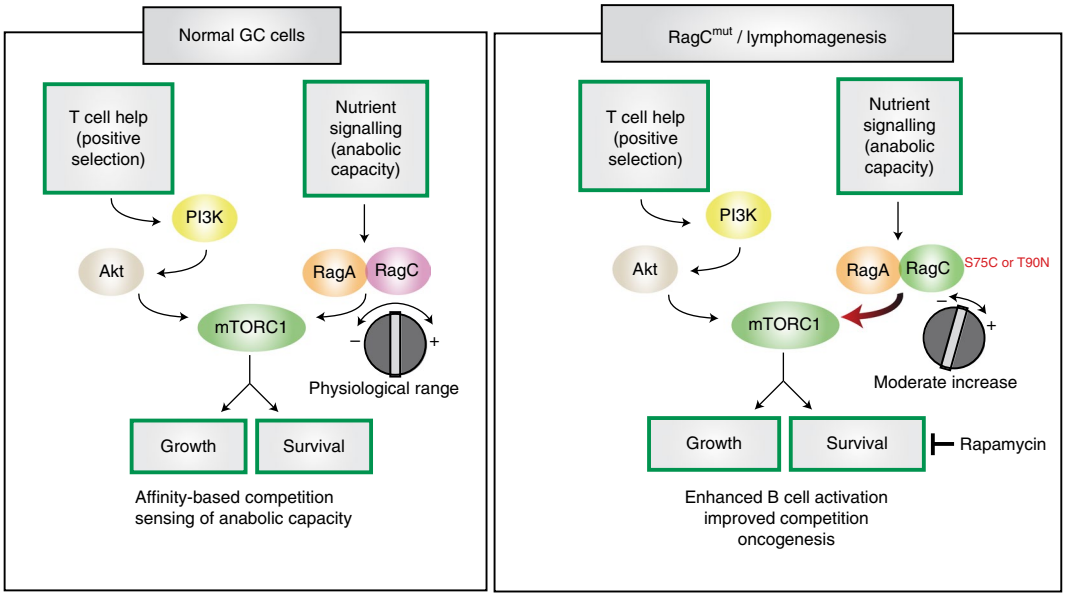

Fig. 6 | Consequences of RagC mutations for GC B cell and lymphomagenesis. The nutrient signalling pathway imposes an 'anabolic capacity' barrier over B-cell activation by T cell help and BCR signalling, so that growth only occurs on nutrient sufficiency. RagC mutations weaken this barrier to allow B cell activation, while still retaining the ability to suppress activation on profound reduction in nutrient levels. During lymphomagenesis, these mutations enhance B cell growth and survival but impose a selective vulnerability to pharmacological inhibition of mTORC1.

activation[36] of RagA showed striking phenotypic aberrations in the B cell lineage and severe impairment of B cell competitiveness in the GC and, consequently, of the entire antibody response. This was paradoxical, given that strong physiological activation of mTORC1 was a requirement for positive selection of GC B cells. Our present data clarify this apparent paradox, by showing that more modest activation of the mTORC1 pathway afforded by patient-derived mutations in RagC provides the correct 'dose' of mTORC1 hyperactivation required to increase rather than decrease GC B cell fitness, and suggests an explanation for why gain-of-function mutations in RagA do not arise in primary lymphomas[31]. Thus, the use of genetically engineered mice expressing RagC mutations under endogenous control and physiological levels revealed an exquisite sensitivity of B cells to different degrees of activation in the nutrient signalling pathway. The sudden burst of growth and proliferation that occurs on B cell activation during the GC reaction, driven by c-myc, PI3K–Akt and NF-κB[36,38,39,46,54,55], among other pathways, depends on an adequate nutrient and energetic supply to sustain the associated anabolic needs. Hence, proper sensing of nutrient sufficiency is imperative to match the extent of the burst to nutrient availability and anabolic capacity, while mismatches caused by excessive activation of the mTORC1 pathway would lead to loss of competitiveness. In this regard, a complete inability to integrate nutrient-level cues in the control of mTORC1 could result in an energetic catastrophe during anabolism and proliferation, whereas a mild increase in nutrient signalling may offer a competitive advantage, if still retaining the ability to respond to dramatic fluctuations in nutrient levels, as oncogenic mutations in *RRAGC* do.

It was recently shown that GC B cells are intrinsically resistant to activation of mTORC1 in response to T cell help via the PI3K–Akt axis, at least when compared with naïve B cells[46]. The two independent arms upstream of mTORC1—PI3K–Akt downstream of BCR and Tfh cell help and activating mutations in the nutrient sensing pathway—significantly synergize, but do not substitute each other (Fig. 6). As predicted, given the decreased requirement for T cell-mediated signals for B cell activation, RagC mutations correlated with decreased presence of Tfh cells ($PD1^+$ T lymphocytes) in both RagC mutant FL samples and human *RRAGC* mutant FL samples (Fig. 5).

We found little evidence of direct control of mTORC1 over proliferation of GC B cells in vivo, consistent with previous results from us and others[36,56,57], albeit more proliferating GC cells were present in RagC mutant mice at all times due to the extraordinary enlargement of the GC B cell population. Transcriptional profiling and functional experiments in GC B cells support a role for RagC mutations in the suppression of apoptosis, even when the anti-apoptotic protein BCL2 was overexpressed (Fig. 5). We postulate that increased mTORC1 activity reinforces B cell activation by T cell help, and suppression of apoptosis is one of the outcomes of B cell activation, probably a critical one in the long process of follicular lymphomagenesis, but not the only one. Indeed, when FL-bearing mice were treated with rapamycin, we observed a selective extension of survival that occurred with a decrease in proliferation of RagC mutant FL cells (Fig. 2), and without a significant increase in C-c3 positive cells. This could be indicative of increased resistance to programmed cell death in established lymphomas when compared with GC B cells, including those GC B cells that overexpress Bcl2. It is also consistent with an early induction of apoptosis with rapid turnover on pharmacological inhibition of mTORC1, followed by a halt in proliferation among remaining viable cells, in line with the well-established cytostatic effects of mTORC1 inhibitors.

Loss-of-function mutation or deletion of *TNFRSF14* in FL induces a supportive microenvironment that includes abundant Tfh[14], which would be partially redundant with *RRAGC* mutations if they confer some degree of independence from Tfh signals. Indeed, mutual exclusiveness of *RRAGC* and *TNFRSF14* mutations was precisely what we observed when we performed a meta-analysis of available mutational data on *RRAGC* and *TNFRSF14* (Fig. 5). It will be worthwhile to evaluate the interplay between the supportive FL microenvironment, as an inheritance of the requirements of GC B cells, and the autochthonous immune response against FL.

Altogether, we demonstrate that a mild increase in nutrient signalling upstream of mTORC1 has dramatic consequences for FL development and sensitizes toward mTORC1 inhibitors. Our work suggests that pharmacological inhibition of mTORC1 with rapalogs or ATP-competitive inhibitors may be particularly efficacious for the 15% of FL harbouring activating mutations in the nutrient signalling pathway. This percentage may be an underestimation, if other genetic lesions or epigenetic means of activating the nutrient signalling pathway are at work in FL patients without *RRAGC*

mutations. Clinical trials with rapalogs as monotherapy have been performed recently in FL[58–60], with a fraction of patients showing impressive responses. These intriguing clinical observations, viewed in the context of our work and the existence of oncogenic mutations in *RRAGC*, trigger speculative thoughts, such as whether the biologic underpinnings of the mTOR dependencies and drug response in FL may be determined precisely, at least in part, by the mutational status of genes involved in this nutrient sensing.

It remains to be determined whether non-genetic perturbations in nutrient signalling (as in the case of chronically increased or decreased nutrient levels) would significantly impact the biology of GC and FL cells. Epidemiology-based connection between elevated nutrient intake, body mass index and B cell lymphoma is far from clear, with reports showing opposite conclusions[61–64]. The humoral response is affected by body mass index in humans and rodents[65,66]. Hence, further research is needed to examine if therapeutic manipulation of nutrient levels may serve as a means of modulating the humoral response and, indeed, if this provides a novel strategy against FL tumours.

Methods

Generation of RagC CRISPR-edited KI mice. To introduce the patient-derived *RRAGC* mutations, C57BL/6 mouse blastocysts were injected with Cas9 mRNA, a single-guide RNA (sgRNA) targeting the sequence of interest (mouse *Rragc)* and a single-stranded DNA oligonucleotide (ssDNA) containing the desired mutation flanked by 40–60 bases homologous to the sequence adjoining the DNA double-strand break. Following clone selection, genotyping was performed by specific PCR followed by restriction fragment length polymorphism or Sanger sequencing.

Sequences used:

For RagC-S74C: TCC→AAC

ssDNA: CGGCCCGGGCGGCGCTGACAGCTCCAAGCCGAGGATCCTGC TTATGGGGCTCCGGCGCAGCGGCAAAAACAGTATCCAAA**AAg**tgagcgcccc gcagccgccgcctgccctggttttgcccggcccacggcgctcaggtggcgggt

gRNA: CGGCAAATCCTCCATCCAGA

For RagC-T89N: ACT→AAT

ssDNA

cttgtatagttaaatagttacaaagttgtctctgtttctcctcacagGTGGTGTTTCATAAGATGTC ACCCAATGAGAATCTGTTCC**TAG**AAAGTACCAACAAGATTTATAAAGATG ACATTTCCAACAGCTCCTTTGTGAACTTCCA

gRNA: ACCCAATGAGACTCTCTTTT

Mice. All animal procedures carried out at the CNIO were performed according to protocols approved by the CNIO-ISCIII Ethics Committee for Research and Animal Welfare (CEIyBA). Ighm$^{\mu MT}$ mice[37] were obtained from Jackson Laboratories (JAX stock no. 002288). Mice were housed under specific pathogen-free conditions at 22 °C and with 12-h dark/light cycles (light cycle from 8:00 to 20:00). Mice were fed with a standard chow diet (Harlan Teklad 2018). All mice were observed weekly by trained personnel. On signs of morbidity, mice were closely inspected daily until application of humane end-point criteria (http://dels.nas.edu/global/ilar/Guide) in consultation with veterinary staff. From our experience, the humane end point is applied when the life expectancy of the mice is, on average, shorter than one week. No maximal tumour volume criteria were used because health decline caused by FL always precedes the growth of measurable bulky tumours. Rapamycin was supplied encapsulated in chow diet at 42 ppm (Rapamycin Holdings and Purina Lab Diet).

Immunizations and mouse experimentation. For the generation of GC response, 8–10-week-old mice were immunized by intraperitoneal (i.p.) injection of (1×10^9) SRBC (Oxoid, catalogue no. SR0053B) in PBS or 50 µg of 4-hydroxy-3-nitrophenylacetyl conjugated to keyhole limpet haemocyanin (NP-KLH, BioSearch, catalogue no. N-5060-5) in alum adjuvant (Thermo Scientific, catalogue no. 77161) (2:1) and analysed at day 10.

To generate larger amounts of GC B cells (that is, for gene expression profiling), we did two sequential i.p. SRBC injections (day 0, 5×10^8; day 5, 1×10^9) and collected cells at day 12. This protocol yielded about three to four times more GC B cells (~12–15% of the B cell fraction) than with a single immunization.

For the memory response assays, mice were immunized by intraperitoneal injection of 50 µg of NP-KLH in complete alum adjuvant and blood was collected at day 0, 7, 14 and 28.

To measure proliferation in GC B cells, mice were immunized by intraperitoneal injection of (1×10^9) SRBC, and after 10 d, 2 h before sacrifice, mice were injected intraperitoneally with 0.5 mg of 5-ethynyl-2′-deoxyuridine (EdU). Analysis of incorporation of EdU was performed using the Click-iT Plus EdU Alexa Fluor 647 Flow Cytometry Assay Kit (Life Technologies, catalogue no. C10634) following the manufacturer's instructions.

For anti-CD40L-induced apoptosis, mice were immunized by intraperitoneal injection of (1×10^9) SRBC, and after 10 d, mice were injected intravenously with 200 µg of anti-CD40L agonist antibody (BioXCell, clone FGK4.5).

To study the effect of rapamycin in GC formation, 10–12-week-old chimeric mice were immunized by intraperitoneal injection of (1×10^9) SRBC and simultaneously treated with encapsulated rapamycin chow diet for 10 d (see Mice) or administered i.p. at 2 mg kg^{-1} at day 8, before assessment of GC formation by flow cytometry at day 10 (see Supplementary Fig. 3d).

Diagnose of murine lymphomas and autoimmunity. Lymphoproliferative diseases developing in the VavP-Bcl2^{tg}; RagC^{mut} cohort were diagnosed based on morphology according to the following criteria, analagous to the classification of human lymphoma: (1) early stages of FL (FL in situ), defined by the presence of oversized follicles with partial or absent mantle zone and loss of confinement in the context of a yet-preserved tissue architecture; (2) overt FL of various grades, characterized by the effacement of the nodal and/or splenic architecture by a proliferation of follicle centre B cells, with a follicular growth pattern occupying the medullary and/or paracortical areas; (3) DLBCL, defined by the effacement of the lymphoid organ architecture due to the expansion of large cells, with occasional infiltration beyond the capsule into surrounding soft tissues[67]. FL was classified into the following three histological grades: grade I, 0–5 centroblasts in ×40 field; grade II, 6–15 centroblasts in ×40 field; grade III, >15 centroblasts in ×40 field. Lymph nodes, spleen, bone marrow and other tissues with abnormal mononuclear infiltrate were evaluated. Mice showing numerous grossly enlarged and fused germinal centres replete with more than five germinal centres per nodule of white pulp in the spleen were considered lymphoma. Bcl6 stain was used in doubtful cases to highlight the follicular pattern. The genotype of the animal was not disclosed to the pathologist (A. de Martino and E. Caleiras). Autoimmunity was scored by perivascular inflammatory infiltrate, predominantly mononuclear of lymphoid aspect, with or without necrosis of the vessel wall, and was most prevalently seen in salivary glands and kidney. Autoimmune glomerulonephritis was defined by hypercellular glomeruli containing eosinophilic deposits, generally accompanied by Bowman epithelium hyperproliferation (a representative example is shown in Supplementary Fig. 2d).

Signalling in MEFs. For amino acid deprivation experiments, subconfluent cell cultures were rinsed twice and incubated in RPMI (US Biological, catalogue no. R8999-04A) and supplemented with 10% dialysed foetal bovine serum (FBS) and all 20 amino acids during 1 h. After that, cells were rinsed three times and placed in RPMI without amino acids, arginine or leucine, and supplemented with 10% dialysed FBS during the indicated time points. Re-stimulation with amino acids was performed over 10 min.

mTORC1 activity in naïve B cells. To study mTORC1 activity in naïve B cells, we isolated CD43$^-$ resting B cells from 8–10-week-old non-immunized mice using magnetic beads, (Myltenyi, catalogue no. 130-049-801) following the manufacturer's instructions. The CD43$^-$ resting B cells (1×10^6) were plated with B cell media: RPMI (US Biological, catalogue no. R8999-04A) + 10% dialysed FBS + 55 µM β-mercaptoethanol (Gibco, catalogue no. 31350-010) + 10 mM HEPES (Lonza, catalogue no. BE17-737E) + 100 µg ml^{-1} penicillin/streptomycin (Gibco, catalogue no. 15070-063) containing no amino acids, with or without cytokines (1 µg ml^{-1} anti-CD40 (R&D Systems, catalogue no. MAB440) and 25 ng ml^{-1} mouse interleukin-4 (R&D Systems, catalogue no. 404-ML)) during 1 h. After this time, stimulation with amino acids was performed for 30 min and cells where collected and processed for flow cytometry.

Class-switch recombination and differentiation in vitro. To study the process of class-switch recombination and plasma cell differentiation in activated mouse B cells, we isolated CD43$^-$ resting B cells from 8−10-week-old non-immunized mice using magnetic beads (Myltenyi, catalogue no. 130-049-801) following the manufacturer's instructions. Cells were washed and resuspended in B cell medium: RPMI (Sigma, catalogue no. R8758) + 10% FBS (Hyclone, catalogue no. SV30160.03) + 55 µM β-mercaptoethanol + 10 mM HEPES + 100 µg ml^{-1} penicillin/streptomycin containing 1 µg ml^{-1} anti-CD40 and 25 ng ml^{-1} mouse interleukin-4. The culture medium was replenished every two days to avoid exhaustion. Four days later, cells were collected and processed for flow cytometry analysis.

To study PRDM1 expression in activated B cells, after 4 d of differentiation, cells were collected and processed for flow cytometry using Alexa Fluor-647 anti-mouse Blimp-1 detection kit (Biolegend, catalogue no. 149902).

To study the effect of rapamycin in plasma cell production, B cells were treated with 1 nM or 10 nM 48 h before collection and flow cytometry analysis (day 4).

B cell proliferation. To study cell proliferation in activated B cells, CD43$^-$ resting B cells were labelled with 5 mM CFSE (Life Technologies, catalogue no. C34554) following the manufacturer's instructions. This reagent monitors distinct generations of proliferating cells by a fluorescent dye dilution. Data were acquired at days 2–4 on a FACSCanto II (BD Biosciences) flow cytometer with 488-nm excitation and an emission filter in the 530/30 nm. Alternatively, analysis of EdU incorporation in 3-d activated B cells was performed using the Click-iT Plus EdU Alexa Fluor 647

Flow Cytometry Assay Kit (Life Technologies, catalogue no. C10634) following the manufacturer's instructions. To study the effect of rapamycin in B cell proliferation, B cells were treated with 1 nM or 10 nM 24 h before the addition of EdU (day 3).

Staining and flow cytometry analysis. Mononuclear cell pools were isolated from mouse spleens at the indicated times postimmunization. Cells were separated by crushing the spleens through a 70-µm mesh (Corning) in ice-cold PBS with 0.1% BSA and 3 mM EDTA, and red blood cells were lysed using Erythrocyte Lysis Buffer (Qiagen, catalogue no.79217). Cell staining was performed on ice in PBS with 0.1% BSA and 3 mM EDTA. We included a prior step of incubation with Fc-block Reagent (Anti-CD16/CD32, Pharmigen, catalogue no. 553142). GC B cells were identified within the B cell fraction ($B220^+$) as $GL7^+$ $CD95^+$. Alternatively, GC B cells were identified within the $CD19^+$ cell fraction, as $CD95^+CD38^-$. Plasma cells were identified by gating on $CD138^+$, $B220^{low}$ cells. Granulocytes were identified as $B220^-/CD4^-/CD8^-/CD11b^-/Gr\text{-}1^+$. Myeloid-derived suppressor cells were identified as $B220^-/CD4^-/CD8^-/CD11b^+/Gr\text{-}1^+$. Myeloid cells were identified as $B220^-/CD4^-/CD8^-/CD11b^+$. Macrophages were identified as $B220^-/CD4^-/CD8^-/CD11b^{low}/F4/80^+$. Follicular helper T cells (Tfh) were identified as $B220^-/CD4^+/CXCR5^+/PD1^+$. For the detection of phosphorylated S235/236 of S6 with intracellular staining, cell suspensions were fixed and permeabilized using the Cytofix-Cytoperm and Cytoperm-Wash buffers (BD Biosciences, catalogue no. 554714) and subsequently stained for 120 min at room temperature. Complete information on antibodies used in flow cytometry is shown in Supplementary Table 3.

All flow cytometry analyses were done at the Flow Cytometry Facility (CNIO), using BD LSR-Fortessa or BD CantoB cell analysers, running BD FACSDiva software (BD Biosciences). FlowJo software (v.9.8.1 and v.10; TreeStar) was used for data analyses and plot rendering. See Supplementary Fig. 6 for details of the gating strategies.

Immunoblotting. Cells were rinsed once with ice-cold PBS and lysed in ice-cold lysis buffer (50 mM HEPES (pH 7.4), 40 mM NaCl, 2 mM EDTA, 1.5 mM sodium orthovanadate, 50 mM NaF, 10 mM pyrophosphate, 10 mM glycerophosphate and 1% Triton X-100 and one tablet of EDTA-free complete protease inhibitors (Roche) per 25 ml). Cell lysates were cleared by centrifugation at 13,000 r.p.m. for 10 min. Protein extracts were denatured by the addition of sample buffer, boiled for 5 min, resolved by SDS–PAGE and analysed by immunoblotting. Western blot analyses were performed according to standard procedures. Antibodies from Cell Signaling Technology were used for detection of P-T389-S6K1 (catalogue no. 9234), S6K1 (catalogue no. 2708), P-S235/236-S6 (catalogue no. 2211), S6 (catalogue no. 2217), P-T37/46-4EBP1 (catalogue no. 2855), 4EBP1 (catalogue no. 9644), P-T308-AKT (catalogue no. 2965), P-S743-AKT (catalogue no. 4060), AKT (catalogue no. 4691). For detection of β-actin we used an antibody from Sigma (catalogue no. A5441).

Gene expression profiling of GC B cells and FL. GC B cells ($B220^+$, $CD95^+$, $CD38^-$) were sorted from $RagC^{mut}$ and $RagC^{wt}$ splenocytes after 12 d of SRBC immunization in a BD FACSAria Ilu (Becton Dickinson) and InFlux (Cytopeia-Becton Dickinson) cell sorters. Total RNA from sorted GC B cells was extracted using TRIzol (Invitrogen, catalogue no. 15596026) and PicoPure RNA Isolation kit (Arcturus, catalogue no. 12204-01) following the manufacturer's instructions. For gene expression profiling of murine lymphomas, $B220^+$ were isolated from mouse lymphoma tumours by immunomagnetic enrichment with CD45R (B220) microbeads (Miltenyi Biotech, catalogue no. 130-049-501).

RagC S74C GC B cell samples. Samples of 500 ng of total RNA were used. The average sample RNA integrity number was 9.75 (range 9.0–10) when assayed on an Agilent 2100 Bioanalyzer. The $poly(A)^+$ fraction was extracted from 1 µg of total RNA, randomly fragmented and converted to double-stranded complementary DNA and processed through subsequent enzymatic treatments of end-repair, dA-tailing and ligation to adaptors, as in the Illumina TruSeq Stranded mRNA Sample Preparation Revision D kit (part no. 15031047; this kit incorporates dUTP during second-strand cDNA synthesis, which implies that only the cDNA strand generated during first-strand synthesis is eventually sequenced). The adapter-ligated library was completed by PCR with Illumina PE primers. The resulting purified cDNA library was applied to an Illumina flow cell for cluster generation and sequenced on an Illumina instrument (Illumina HiSeq2500) by following the manufacturer's protocols. Image analysis, per cycle base calling and quality score assignment were performed with Illumina Real Time Analysis software. Conversion of Illumina BCL files to bam format was performed with the Illumina2bam tool (Wellcome Trust Sanger Institute New Pipeline Group (NPG); https://github.com/wtsi-npg/illumina2bam).

RagC T89N GC B and RagC S74C FL samples. Samples of 500 ng of total RNA (but 100 ng for YRT-236, and 200-300 ng for YRT-224, -230 and -235) were used. Average sample RNA integrity number was 8.5 (range 7.9–10) when assayed on an Agilent 2100 Bioanalyzer. The $poly(A)^+$ fraction was purified and randomly fragmented, converted to double-stranded cDNA and processed through subsequent enzymatic treatments of end-repair, dA-tailing and ligation to adaptors as in the NEBNext Ultra II Directional RNA Library Prep Kit for Illumina (NEB, catalogue no. E7760) (this kit incorporates dUTP during second-strand cDNA synthesis, which implies that only the cDNA strand generated during first-strand synthesis is eventually sequenced). The adapter-ligated library was completed by PCR with Illumina PE primers. The resulting purified cDNA library was applied to an Illumina flow cell for cluster generation and sequenced on an Illumina instrument (Illumina HiSeq2500) following the manufacturer's protocols. Image analysis, per cycle base calling and quality score assignment were performed with Illumina Real Time Analysis software. Conversion of BCL files to FASTQ format was performed with the bcl2fastq Software (Illumina).

Sequencing reads were analysed with the nextpresso pipeline (http://bioinfo.cnio.es/nextpresso/) as follows: sequencing quality was checked with FastQC v.0.11.0 (http://www.bioinformatics.babraham.ac.uk/projects/fastqc/). Reads were aligned to the mouse genome (NCBI37/mm9) with TopHat v.2.0.10 (ref. [68]) using Bowtie v.1.0.0 (ref. [69]) and SAMtools v.0.1.19 (ref. [70]), allowing 2 mismatches and 20 multihits. Differential expression was tested with DESeq2 (ref. [71]), using the mouse NCBI37/mm9 transcript annotations from https://ccb.jhu.edu/software/tophat/igenomes.shtml. GSEA Pre-ranked[35] was used to perform gene-set enrichment analysis of the described gene signatures on a pre-ranked gene list, setting 1,000 gene-set permutations. GSEA Pre-ranked calculates an enrichment score for each gene set using the Kolmogorov–Smirnov test. The nominal *P* value estimates the statistical significance of the enrichment score for a single gene set and it was corrected for gene-set size and multiple hypothesis testing. For GSEA analysis, non-expressed genes were removed from the ranking.

ELISA. Total IgG_1 serum titres after 10 d of SRBC immunization were measured by ELISA using mouse IgG1 ELISA kit (Abcam, catalogue no. ab133045) and following the manufacturer's instructions. High-affinity and total NP-specific antibodies were measured by ELISA using 10 mg ml^{-1} of NP(2.5)-BSA or NP(25)-BSA as the coating reagent, respectively. Serum was assayed in threefold dilutions starting at 1/100. NP-specific IgG1 was detected using goat anti-mouse IgG1 Fc-specific antibody conjugated to horseradish peroxidase (Jackson Immunoresearch, catalogue no. 115-035-071) and developed with tetramethylbenzidine (Sigma, T4319). The optical density OD_{450} was measured using a Synergy4 microplate reader (Izasa Scientific). Titres were calculated by logarithmic interpolation of the dilutions with readings immediately above and immediately below an OD_{450} of 0.2 (for example, if OD_{450} readings at dilution 2 (1/900) = 0.3 and at dilution 3 (1/2,700) = 0.1, then titre = dilution = 2.5 = 1/1,558).

Histological and histochemical analysis of mouse tissues. Tissue samples were fixed in 10% neutral buffered formalin (4% formaldehyde in solution), paraffin embedded and cut at 3 µm, mounted in superfrost plus slides and dried overnight. For different staining methods, slides were deparaffinized in xylene and rehydrated through a series of graded concentrations of ethanol in water. Consecutive sections were stained with haematoxylin and eosin (H&E), and several immunohistochemistry reactions were performed in an automated immunostaining platform (Ventana Discovery XT). Antigen retrieval was first performed with the appropriate pH buffer, (CC1m, Ventana, Roche) and endogenous peroxidase was blocked (peroxide hydrogen at 3%). Then, slides were incubated with the appropriate primary antibody as detailed: rabbit monoclonal anti-PD1 (D7D5W, 1/50, Cell Signaling Technology, catalogue no. 84651), mouse monoclonal anti-Bcl6 (191E/A8; 1/30; CNIO Monoclonal Antibodies Core Unit. catalogue no. AM(191E/A8)) and rabbit polyclonal anti-Cleaved Caspase 3 (1/300, Cell Signaling Technology, catalogue no. 9661). After the primary antibody, slides were incubated with the visualization systems (Omni Map anti-Rabbit, Ventana, Roche) conjugated with horseradish peroxidase. Immunohistochemical reaction was developed using 3,30-diaminobenzidine tetrahydrochloride (DAB) (Chromo Map DAB, Ventana, Roche; DAB Dako) and nuclei were counterstained with Carazzi's haematoxylin. Finally, the slides were dehydrated, cleared and mounted with a permanent mounting medium for microscopic evaluation. Positive control sections known to be primary antibody positive were included for each staining run. For PD1 quantification, whole slides were acquired with a slide scanner (AxioScan Z1, Zeiss). After selection of regions of interest (lymph nodes and spleen), areas for quantification were selected and exported as subsets of images in tiff format. All images were then checked, and those with staining or cutting artefacts were eliminated. Different images from different slides were chosen for quantification programme training (AxioVision v.4.6 software package, Zeiss) and an appropriate script for each antibody was created. For PD1 quantification, positivity was evaluated in one phase (phase 1, positive cells) and compared with total tissue area (phase 2, total cells). After training and script optimization, the quantification programme was run and results exported as Excel files with scoring data for each tiff file. Data obtained were then compiled and appropriately assessed.

Histology and immunohistochemistry FL patient samples. Written consent was obtained for collection and use of patient specimens for research purposes with ethical approval granted by the Health Research Authority: London City and East Research Ethics Committee (REC Ref: 10/H0704/65 and 06/Q0605/69). Immunohistochemistry (IHC) staining was performed in an automated system following the manufacturer's instructions (Leica Bond-Max, Epitope Retrieval Solution 2 AR9640 for 20 min and Bond Polymer Refine Detection DS9800; Leica Microsystems). The primary antibody was a mouse monoclonal anti-PD1, clone NAT105C/E3 lot number 0208, provided by G. Roncador (Monoclonal Antibodies Core Unit, CNIO). Incubation time of the primary antibody was 15 min. The tissue

microarray had three punches per biopsy that were distributed discontinuously. The resulting cores had a diameter of 1–1.5 mm. The PD1 analysis was set up as in refs. [72,73] and was done as follows. First, observation was made using a bright-field Olympus BX63 microscope (Olympus). Then, the slide was scanned at ×400 magnification using a digital pathology system (Hamamatsu NanoZoomer C9600) and visualized with NDP.view2 software (Hamamatsu Photonics). PD1 was quantified on the basis of the expression within the follicles, except when the follicular lymphoma had a completely diffuse pattern. PD1 was measured as 0 (<1%), +1 (1–5%), +2 (5–20%) and +3 (>20%). The analysis of the cores was made without previous knowledge of the mutational status of *RRAGC*. The value of each core was recorded and the average of the three cores was calculated. Occasional broken cores, with insufficient tissue or inadequate immunohistochemical staining, were excluded from the analysis. Comparisons were made by non-parametric Mann–Whitney *U*-test, one-tailed and with a priori significance level of 0.05 (www.socscistatistics.com).

Quantification, statistical analysis and reproducibility. The values of *n*, total number of animals per group, as well as the definition of centre, dispersion and precision measures are reported in each figure and figure legend. Unless otherwise stated, two-sided Student's *t*-test or chi-squared tests were performed as depicted in the figures. Survival in mouse experiments was represented with Kaplan–Meier curves, and significance was estimated with the log-rank test. Analyses were carried out using Prism software (GraphPad). Further information on statistical parameters, software, study design and reagents used can be found in the Reporting Summary.

Reproducibility. The experiments in Fig. 1a were performed four times independently for RagC$^{S74C/+}$ mice and three times independently for RagC $^{T89N/+}$ mice showing similar results. The experiments quantified in Supplementary Fig. 1f were performed seven times independently for RagC$^{S74C/+}$ mice and four times independently for RagC $^{T89N/+}$ mice showing similar results. The experiments in Fig. 1b were performed three times independently per genotype showing similar results. The experiments in Fig. 1d were performed eight times independently in RagC$^{S74C/+}$B cells, two times independently in RagC$^{T89N/+}$ B cells and one time in RagA B cells showing similar results. The experiments in Fig. 1e were performed two times independently per genotype showing similar results. The experiment in Supplementary Fig. 1g was performed once for each genotype. The experiment in Supplementary Fig. 1h was performed once. The experiment in Fig. 2a,c–e,g–j was performed once. The experiment in Supplementary Fig. 2a was performed two times independently for each genotype. The experiment in Supplementary Fig. 2b,f,g,j,i,l was performed once. The experiment in Supplementary Fig. 2k was performed two independent times showing similar results. The experiments in Fig. 3a were performed 19 times independently in RagC$^{S74C/+}$ mice and 14 times independently in RagC$^{T89N/+}$ mice showing similar results. The experiments in Fig. 3b were performed four times independently in RagC$^{S74C/+}$ mice and three times independently in RagC$^{T89N/+}$ showing similar results. The experiments in Fig. 3c were performed two times independently in both strains showing similar results. The experiments in Fig. 3d were performed one time in the RagC$^{S74C/+}$ mice and two times independently in RagC$^{T89N/+}$ mice showing similar results. The experiments in Fig. 3e were performed once. The experiments in Fig. 3f were performed two times independently in VavP-Bcl2^{tg}; RagC$^{S74C/+}$ and Bcl2^{tg}; RagC$^{T89N/+}$ mice showing similar results. The experiments in Supplementary Fig. 3b were performed twice in each genotype showing similar results.

The experiment in Supplementary Fig. 3c was performed twice showing similar results. The experiments in Supplementary Fig. 3d were performed three times showing similar results. The experiments in Fig. 4b–d and Supplementary Fig. 4a–c were performed once. The experiments in Fig. 4f,g,j were performed two times independently showing similar results. The experiments in Fig. 4h and Supplementary Fig. 4h,i were performed three times independently showing similar results. The experiments in Fig. 4l,m and Supplementary Fig. 4d were performed two times independently for RagC$^{S74C/+}$ mice and once for RagC$^{T89N/+}$ mice showing similar results. The experiment in Supplementary Fig. 4f was performed once. The experiments in Supplementary Fig. 4j were performed two times independently for each genotype showing similar results. The experiments in Fig. 5a and Supplementary Fig. 5a–c were each performed once. The experiments in Fig. 5b and Supplementary Fig. 5e were performed five times independently in RagC$^{S74C/+}$ mice and two times independently in RagC$^{T89N/+}$ mice showing similar results. The experiments in Fig. 5d were performed three times independently for each genotype showing similar results. The experiments in Fig. 5e–g were performed once. The results obtained in Fig. 5h were validated on a different cohort of FL patients (Supplementary Fig. 5k). The experiments in Supplementary Fig. 5d were performed four times independently in RagC$^{S74C/+}$ mice and five times independently in RagC$^{T89N/+}$ mice showing similar results. The experiments in Supplementary Fig. 5f,g,j were performed two times independently showing similar results.

Reporting Summary. Further information on research design is available in the Nature Research Reporting Summary linked to this article.

Data availability

Sequence data that support the findings of this study have been deposited in GEO, with the accession codes GSE125393 and GSE125394. The data that support the findings of this study are available from the corresponding author upon request. The data that support the plots within this paper and other findings of this study are available from the corresponding author upon reasonable request.

Received: 4 February 2019; Accepted: 12 July 2019;
Published online: 19 August 2019

References

1. Kahl, B. D. & Yang, D. T. Follicular lymphoma: evolving therapeutic strategies. *Blood* **127**, 2055–2063 (2016).
2. Victora, G. D. & Nussenzweig, M. C. Germinal centers. *Annu. Rev. Immunol.* **30**, 429–457 (2012).
3. Shlomchik, M. J. & Weisel, F. Germinal center selection and the development of memory B and plasma cells. *Immunol. Rev.* **247**, 52–63 (2012).
4. Mesin, L., Ersching, J. & Victora, G. D. Germinal center B cell dynamics. *Immunity* **45**, 471–482 (2016).
5. Bannard, O. & Cyster, J. G. Germinal centers: programmed for affinity maturation and antibody diversification. *Curr. Opin. Immunol.* **45**, 21–30 (2017).
6. Tas, J. et al. Visualizing antibody affinity maturation in germinal centers. *Science* **351**, 1048–1054 (2016).
7. de Jong, D. & Fest, T. The microenvironment in follicular lymphoma. *Best Pract. Res. Clin. Haematol.* **24**, 135–146 (2011).
8. Huet, S., Sujobert, P. & Salles, G. From genetics to the clinic: a translational perspective on follicular lymphoma. *Nat. Rev. Cancer* **18**, 224–239 (2018).
9. Pasqualucci, L. et al. Genetics of follicular lymphoma transformation. *Cell Rep.* **6**, 130–140 (2014).
10. Pasqualucci, L. et al. Inactivating mutations of acetyltransferase genes in B-cell lymphoma. *Nature* **471**, 189–195 (2011).
11. Morin, R. D. et al. Frequent mutation of histone-modifying genes in non-Hodgkin lymphoma. *Nature* **476**, 298–303 (2011).
12. Morin, R. D. et al. Somatic mutations altering EZH2 (Tyr641) in follicular and diffuse large B-cell lymphomas of germinal-center origin. *Nat. Genet.* **42**, 181–185 (2010).
13. Okosun, J. et al. Integrated genomic analysis identifies recurrent mutations and evolution patterns driving the initiation and progression of follicular lymphoma. *Nat. Genet* **46**, 176–181 (2014).
14. Boice, M. et al. Loss of the HVEM tumor suppressor in lymphoma and restoration by modified CAR-T cells. *Cell* **167**, 405–418 (2016).
15. Challa-Malladi, M. et al. Combined genetic inactivation of *β2-microglobulin* and *CD58* reveals frequent escape from immune recognition in diffuse large B cell lymphoma. *Cancer Cell* **20**, 728–740 (2011).
16. Cheung, K. J. J. et al. Acquired *TNFRSF14* mutations in follicular lymphoma are associated with worse prognosis. *Cancer Res.* **70**, 9166–9174 (2010).
17. Kridel, R. et al. Histological transformation and progression in follicular lymphoma: a clonal evolution study. *PLoS Med.* **13**, e1002197 (2016).
18. Launay, E. et al. High rate of TNFRSF14 gene alterations related to 1p36 region in de novo follicular lymphoma and impact on prognosis. *Leukemia* **26**, 559–562 (2012).
19. Ying, Z. X. et al. Recurrent mutations in the MTOR regulator RRAGC in follicular lymphoma. *Clin. Cancer Res.* **22**, 5383–5393 (2016).
20. Okosun, J. et al. Recurrent mTORC1-activating RRAGC mutations in follicular lymphoma. *Nat. Genet.* **48**, 183–188 (2016).
21. Green, M. R. et al. Mutations in early follicular lymphoma progenitors are associated with suppressed antigen presentation. *Proc. Natl Acad. Sci. USA* **112**, E1116–E1125 (2015).
22. Ben-Sahra, I. & Manning, B. D. mTORC1 signaling and the metabolic control of cell growth. *Curr. Opin. Cell Biol.* **45**, 72–82 (2017).
23. Efeyan, A., Comb, W. C. & Sabatini, D. M. Nutrient-sensing mechanisms and pathways. *Nature* **517**, 302–310 (2015).
24. Kim, E., Goraksha-Hicks, P., Li, L., Neufeld, T. P. & Guan, K. L. Regulation of TORC1 by Rag GTPases in nutrient response. *Nat. Cell Biol.* **10**, 935–945 (2008).
25. Sancak, Y. et al. The Rag GTPases bind raptor and mediate amino acid signaling to mTORC1. *Science* **320**, 1496–1501 (2008).
26. Shen, K., Choe, A. & Sabatini, D. M. Intersubunit crosstalk in the Rag GTPase heterodimer enables mTORC1 to respond rapidly to amino acid availability. *Mol. Cell* **68**, 552–565 (2017).
27. Shimobayashi, M. & Hall, M. N. Making new contacts: the mTOR network in metabolism and signalling crosstalk. *Nat. Rev. Mol. Cell Biol.* **15**, 155–162 (2014).
28. Valvezan, A. J. & Manning, B. D. Molecular logic of mTORC1 signalling as a metabolic rheostat. *Nat. Metab.* **1**, 321–333 (2019).
29. Tsun, Z. Y. et al. The folliculin tumor suppressor is a GAP for the RagC/D GTPases that signal amino acid levels to mTORC1. *Mol. Cell* **52**, 495–505 (2013).
30. Wang, H. et al. One-step generation of mice carrying mutations in multiple genes by CRISPR/cas-mediated genome engineering. *Cell* **153**, 910–918 (2013).
31. Efeyan, A. et al. Regulation of mTORC1 by the Rag GTPases is necessary for neonatal autophagy and survival. *Nature* **493**, 679–683 (2013).

32. Hara, K. et al. Amino acid sufficiency and mTOR regulate p70 S6 kinase and eIF-4E BP1 through a common effector mechanism. *J. Biol. Chem.* **273**, 14484–14494 (1998).
33. Wang, S. et al. Metabolism. Lysosomal amino acid transporter SLC38A9 signals arginine sufficiency to mTORC1. *Science* **347**, 188–194 (2015).
34. Egle, A., Harris, A. W., Bath, M. L., O'Reilly, L. & Cory, S. VavP-Bcl2 transgenic mice develop follicular lymphoma preceded by germinal center hyperplasia. *Blood* **103**, 2276–2283 (2004).
35. Subramanian, A. et al. Gene set enrichment analysis: a knowledge-based approach for interpreting genome-wide expression profiles. *Proc. Natl Acad. Sci. USA* **102**, 15545–15550 (2005).
36. Ersching, J. et al. Germinal center selection and affinity maturation require dynamic regulation of mTORC1 kinase. *Immunity* **46**, 1045–1058 (2017).
37. Kitamura, D., Roes, J., Kuhn, R. & Rajewsky, K. A. B cell-deficient mouse by targeted disruption of the membrane exon of the immunoglobulin μ chain gene. *Nature* **350**, 423–426 (1991).
38. Calado, D. P. et al. The cell-cycle regulator c-Myc is essential for the formation and maintenance of germinal centers. *Nat. Immunol.* **13**, 1092–1100 (2012).
39. Dominguez-Sola, D. et al. The proto-oncogene MYC is required for selection in the germinal center and cyclic reentry. *Nat. Immunol.* **13**, 1083–1091 (2012).
40. Krysiak, K. et al. Recurrent somatic mutations affecting B-cell receptor signaling pathway genes in follicular lymphoma. *Blood* **129**, 473–483 (2017).
41. Peng, T., Golub, T. R. & Sabatini, D. M. The immunosuppressant rapamycin mimics a starvation-like signal distinct from amino acid and glucose deprivation. *Mol. Cell Biol.* **22**, 5575–5584 (2002).
42. Murakami, M. et al. mTOR is essential for growth and proliferation in early mouse embryos and embryonic stem cells. *Mol. Cell. Biol.* **24**, 6710–6718 (2004).
43. Thoreen, C. C. et al. An ATP-competitive mammalian target of rapamycin inhibitor reveals rapamycin-resistant functions of mTORC1. *J. Biol. Chem.* **284**, 8023–8032 (2009).
44. Feldman, M. E. et al. Active-site inhibitors of mTOR target rapamycin-resistant outputs of mTORC1 and mTORC2. *PLoS Biol.* **7**, e38 (2009).
45. Zoncu, R., Efeyan, A. & Sabatini, D. M. mTOR: from growth signal integration to cancer, diabetes and ageing. *Nat. Rev. Mol. Cell Biol.* **12**, 21–35 (2011).
46. Luo, W., Weisel, F. & Shlomchik, M. J. B. B cell receptor and CD40 signaling are rewired for synergistic induction of the c-Myc transcription factor in germinal center B cells. *Immunity* **48**, 313–326 (2018).
47. Han, S. et al. Cellular interaction in germinal centers. Roles of CD40 ligand and B7-2 in established germinal centers. *J. Immunol.* **155**, 556–567 (1995).
48. Papa, I. & Vinuesa, C. G. Synaptic interactions in germinal centers. *Front. Immunol.* **9**, 1858 (2018).
49. Vinuesa, C. G. & Cyster, J. G. How T cells earn the follicular rite of passage. *Immunity* **35**, 671–680 (2011).
50. Vinuesa, C. G., Linterman, M. A., Yu, D. & MacLennan, I. C. M. Follicular helper T cells. *Annu. Rev. Immunol.* **34**, 335–368 (2016).
51. Qi, H., Cannons, J. L., Klauschen, F., Schwartzberg, P. L. & Germain, R. N. SAP-controlled T–B cell interactions underlie germinal centre formation. *Nature* **455**, 764–769 (2008).
52. Zoncu, R. et al. mTORC1 senses lysosomal aminoacids through an inside-out mechanism that requires the vacuolar H^+-ATPase. *Science* **334**, 678–683 (2011).
53. Efeyan, A. et al. RagA, but not RagB, is essential for embryonic development and adult mice. *Dev. Cell* **29**, 321–329 (2014).
54. Boothby, M. & Rickert, R. C. Metabolic regulation of the immune humoral response. *Immunity* **46**, 742–755 (2017).
55. Heise, N. et al. Germinal center B cell maintenance and differentiation are controlled by distinct NF-κB transcription factor subunits. *J. Exp. Med.* **211**, 2103–2118 (2014).
56. Dowling, R. J. O. et al. mTORC1-mediated cell proliferation, but not cell growth, controlled by the 4E-BPs. *Science* **328**, 1172–1176 (2010).
57. Barbet, N. C. et al. TOR controls translation initiation and early G1 progression in yeast. *Mol. Biol. Cell* **7**, 25–42 (1996).
58. Smith, S. M. et al. Temsirolimus has activity in non-mantle cell non-Hodgkin's lymphoma subtypes: The University of Chicago phase II consortium. *J. Clin. Oncol.* **28**, 4740–4746 (2010).
59. Bannani, N. N. et al. Efficacy of the oral mTORC1 inhibitor everolimus in relapsed or refractory indolent lymphoma. *Am. J. Hematol.* **92**, 448–453 (2017).
60. Witzig, T. E. et al. A phase II trial of the oral mTOR inhibitor everolimus in relapsed aggressive lymphoma. *Leukemia* **25**, 341–347 (2011).
61. Willett, E. V. et al. Non-Hodgkin lymphoma and obesity: a pooled analysis from the InterLymph Consortium. *Int. J. Cancer* **122**, 2062–2070 (2008).
62. Renehan, A. G., Tyson, M., Egger, M., Heller, R. F. & Zwahlen, M. Body-mass index and incidence of cancer: a systematic review and meta-analysis of prospective observational studies. *Lancet* **371**, 569–578 (2008).
63. Bhaskaran, K. et al. Body-mass index and risk of 22 specific cancers: a population-based cohort study of 5.24 million UK adults. *Lancet* **384**, 755–765 (2014).
64. The Global BMI Mortality Collaboration Body-mass index and all-cause mortality: individual-participant-data meta-analysis of 239 prospective studies in four continentsThe Global BMI Mortality Collaboration †Show footnotes. *Lancet* **388**, 776–786 (2016).
65. Kosaraju, R. et al. B cell activity is impaired in human and mouse obesity and is responsive to an essential fatty acid upon murine influenza infection. *J. Immunol.* **198**, 4738–4752 (2017).
66. Sheridan, P. A. et al. Obesity is associated with impaired immune response to influenza vaccination in humans. *Int. J. Obes. (Lond.)* **36**, 1072–1077 (2012).
67. Zhang, J. et al. The CREBBP acetyltransferase is a haploinsufficient tumor suppressor in B-cell lymphoma. *Cancer Discov.* **7**, 322–337 (2017).
68. Trapnell, C. et al. Differential gene and transcript expression analysis of RNA-seq experiments with TopHat and Cufflinks. *Nat. Protoc.* **7**, 562–578 (2012).
69. Langmead, B., Trapnell, C., Pop, M. & Salzberg, S. Ultrafast and memory-efficient alignment of short DNA sequences to the human genome. *Genome Biol.* **10**, R25 (2009).
70. Li, H. et al. The Sequence Alignment/Map format and SAMtools. *Bioinformatics* **25**, 2078–2079 (2009).
71. Love, M. I., Huber, W. & Anders, S. Moderated estimation of fold change and dispersion for RNA-seq data with DESeq2. *Genome Biol.* **15**, 550 (2014).
72. Carreras, J. et al. High numbers of tumor-infiltrating programmed cell death 1-positive regulatory lymphocytes are associated with improved overall survival in follicular lymphoma. *J. Clin. Oncol.* **27**, 1470–1476 (2009).
73. Carreras, J. et al. Genomic profile and pathologic features of diffuse large b-cell lymphoma subtype of methotrexate-associated lymphoproliferative disorder in rheumatoid arthritis patients. *Am. J. Surg. Pathol.* **42**, 936–950 (2018).

Acknowledgements

We are indebted to D. M. Sabatini (R01 CA129105, R01 CA103866 and R37 AI047389) and thank R. Jaenisch, S. Markoulaki and the Whitehead Institute for Biomedical Research CRISPR facility for zygote injections. We thank A. Clear and K. Korfi for generating TMAs from lymphoma patients, and P. A. Katajisto for critical reading of the manuscript. We also thank CNIO Flow Cytometry, Histopathology, Animal Facility and Genomics Core Units for excellent technical support. Research was supported by the RETOS projects Programme of Spanish Ministry of Science, Innovation and Universities, Spanish State Research Agency, cofunded by the European Regional Development Fund (grant SAF2015-67538-R), EU-H2020 Programme (ERC-2014-STG-638891), Excellence Network Grant from MICIU/AEI (SAF2016-81975-REDT), a Ramon y Cajal Award from MICIU/AEI (RYC-2013-13546), Spanish Association Against Cancer Research Scientific Foundation Laboratory Grant, Beca de Investigación en Oncología Olivia Roddom, FERO Grant for Research in Oncology; Miguel Servet Fellowship and Grant Award (MS16/00112 and CP16/00112) and Project PI18/00816 within the Health Strategic Action from the ISCIII (to A.O.-M.), both cofunded by the European Regional Development Fund, Marcos Fernandez Fellowship from the Spanish Leukaemia and Lymphoma Foundation/Vistare Foundation (to A.O.-M.) and L'Oreal For Women in Science Award (to A.O.-M.). J.F. is a recipient of a Cancer Research UK Programme Award (15968) and J.O. is a recipient of a Cancer Research UK Clinician Scientist Fellowship (22742). N.M.-M. is a Ramon y Cajal Awardee MICIU/AEI (RYC-2016-20173). N.D.-S., C.C.A., A.B.P.-G. and K.T. are recipients of Ayudas de contratos predoctorales para la formacion de doctores from MICIU/AEI (BES-2016-077410, BES-2015-073776, BES-2017–081381, BES-2016-078082).

Author contributions

A.O.-M. performed most experiments, contributed to experimental design, data analysis and writing of the manuscript. N.D.-S, A.S., C.L.-F, C.M., C.C.A., A.V., L.M.-A, B.F.-R, A.B.P-G. and N.M.-M. provided help with experimentation. K.T. and E.P.-Y. performed bioinformatics analysis of RNA-seq and meta-analysis of mutually exclusive mutations. E.C. and A.D.M. performed and diagnosed the histology and pathology. J.C. and N.N. performed and analysed immunohistochemistry studies on human samples. S.A., J.O. and J.F. performed the mutation analyses on the patient samples, provided the corresponding tissue microarrays and clinical information. J.O., J.F. and G.D.V. contributed critical intellectual input in design and interpretation of data. A.E. conceived and supervised the study, analysed the data, wrote the manuscript and secured funding. All authors read and commented on the manuscript and figures.

Competing interests

The authors declare no competing interests.

Additional information

Supplementary information is available for this paper at https://doi.org/10.1038/s42255-019-0098-8.

Reprints and permissions information is available at www.nature.com/reprints.

Correspondence and requests for materials should be addressed to A.E.

Peer review information: Primary Handling Editor: Ana Mateus.

Publisher's note: Springer Nature remains neutral with regard to jurisdictional claims in published maps and institutional affiliations.

nature research

Corresponding author(s): Alejo Efeyan

Last updated by author(s): Jul 8, 2019

Reporting Summary

Nature Research wishes to improve the reproducibility of the work that we publish. This form provides structure for consistency and transparency in reporting. For further information on Nature Research policies, see Authors & Referees and the Editorial Policy Checklist.

Statistics

For all statistical analyses, confirm that the following items are present in the figure legend, table legend, main text, or Methods section.

n/a	Confirmed	
☐	☒	The exact sample size (*n*) for each experimental group/condition, given as a discrete number and unit of measurement
☐	☒	A statement on whether measurements were taken from distinct samples or whether the same sample was measured repeatedly
☐	☒	The statistical test(s) used AND whether they are one- or two-sided *Only common tests should be described solely by name; describe more complex techniques in the Methods section.*
☒	☐	A description of all covariates tested
☒	☐	A description of any assumptions or corrections, such as tests of normality and adjustment for multiple comparisons
☐	☒	A full description of the statistical parameters including central tendency (e.g. means) or other basic estimates (e.g. regression coefficient) AND variation (e.g. standard deviation) or associated estimates of uncertainty (e.g. confidence intervals)
☐	☒	For null hypothesis testing, the test statistic (e.g. *F*, *t*, *r*) with confidence intervals, effect sizes, degrees of freedom and *P* value noted *Give P values as exact values whenever suitable.*
☒	☐	For Bayesian analysis, information on the choice of priors and Markov chain Monte Carlo settings
☒	☐	For hierarchical and complex designs, identification of the appropriate level for tests and full reporting of outcomes
☒	☐	Estimates of effect sizes (e.g. Cohen's *d*, Pearson's *r*), indicating how they were calculated

Our web collection on statistics for biologists contains articles on many of the points above.

Software and code

Policy information about availability of computer code

Data collection	Odyssey Infrared Imaging System. Application software version 3.0.30. LI-COR Biosciences, NDP.view2 software FlowJo v9.8.1 and v10 AxioScan Z1, Zeiss BD FACSDiva software (BD Biosciences)
Data analysis	GraphPad Prism v5.03; https://www.socscistatistics.com/; AxioVision 4.6 software package

For manuscripts utilizing custom algorithms or software that are central to the research but not yet described in published literature, software must be made available to editors/reviewers. We strongly encourage code deposition in a community repository (e.g. GitHub). See the Nature Research guidelines for submitting code & software for further information.

Data

Policy information about availability of data

All manuscripts must include a data availability statement. This statement should provide the following information, where applicable:

- Accession codes, unique identifiers, or web links for publicly available datasets
- A list of figures that have associated raw data
- A description of any restrictions on data availability

Sequence data that support the findings of this study have been deposited in GEO, with the accession codes GSE125393 and GSE125394

Field-specific reporting

Please select the one below that is the best fit for your research. If you are not sure, read the appropriate sections before making your selection.

☒ Life sciences ☐ Behavioural & social sciences ☐ Ecological, evolutionary & environmental sciences

For a reference copy of the document with all sections, see nature.com/documents/nr-reporting-summary-flat.pdf

Life sciences study design

All studies must disclose on these points even when the disclosure is negative.

Sample size	We did not estimate the sample size calculation for most studies, as the magnitude of the effect sizes were unknown.
Data exclusions	No data were excluded unless as determined by technical problems, such as low RNA quality, low number of cells.
Replication	All attempts of replication were successful.
Randomization	Mice were randomly assigned to different treatments.
Blinding	Whenever possible, and in most experiments, investigators were blinded to genotype as mice have numbered IDs but no information on genotypes is available in cage cards. Genotypes were verified at the analysis step. To diagnose murine lymphomas, the genotype of the mouse was not disclosed to the pathologist.

Reporting for specific materials, systems and methods

We require information from authors about some types of materials, experimental systems and methods used in many studies. Here, indicate whether each material, system or method listed is relevant to your study. If you are not sure if a list item applies to your research, read the appropriate section before selecting a response.

Materials & experimental systems

n/a	Involved in the study
☐	☒ Antibodies
☒	☐ Eukaryotic cell lines
☒	☐ Palaeontology
☐	☒ Animals and other organisms
☐	☒ Human research participants
☒	☐ Clinical data

Methods

n/a	Involved in the study
☒	☐ ChIP-seq
☐	☒ Flow cytometry
☒	☐ MRI-based neuroimaging

Antibodies

Antibodies used

B220 PE-Cy7 RA3-6B2 #561881 BD Pharmingen
B220 BUV737 RA3-6B2 #564449 BD Horizon
CD19 PE 1D3 #557399 BD Pharmingen
GL7 PE GL7 #561530 BD Pharmingen
CD95 FITC Jo2 #561979 BD Pharmingen
CD138 BV421 281-2 #562610 BD Horizon
CD38 AF700 90 #56-0381-82 eBioscience
CD4 FITC GK1.5 #11-0041-81 eBioscience
CD4 BUV395 GK1.5 #563790 BD Horizon
CD8 PE 53-6.7 #553032 BD Pharmingen
CD11b PE-Cy7 M1/70 #561098 BD Pharmingen
Gr-1 FITC RB6-8C5 #562060 BD Pharmingen
F4/80 APCeF780 BM8 #47-4801-80 eBioscience
PRDM1 AF647 5E7 #149902 Biolegend
P-S235/236-S6 AF647 D57.2.2E #4851 Cell Signaling Technology
IgG1 APC A85-1 #560089 BD Pharmingen
CD45.1 PErCP-Cy5.5 A20 #560580 BD Pharmingen
CD45.2 APC-Cy7 104 #109824 Biolegend
CXCR5 Biotin 2G8 #551960 BD Pharmingen
Streptavidin PE #554061 BD Pharmingen
PD-1 PE-Cy7 J43 #25-9985-80 eBioscience
P-T389-S6K1 #9234 Cell Signaling Technology
S6K1 #2708 Cell Signaling Technology
P-T37/46-4EBP1 #2855 Cell Signaling Technology

4EBP1 #9644 Cell Signaling Technology
P-T308-AKT #2965 Cell Signaling Technology
P-S743-AKT #4060 Cell Signaling Technology
AKT #4691 Cell Signaling Technology
β-actin #A5441 Sigma
IgG1 Fc-specific antibody conjugated to horseradish peroxidase # 115-035-071 Jackson Immunoresearch
anti-PD-1 #84651 Cell Signaling Technology
anti-Bcl6 #AM(191E/A8) CNIO Monoclonal Antibodies Core Unit
anti-Cleaved Caspase 3 #9661 Cell Signaling Technology
anti-PD-1 NAT105C/E3 lot num. 0208 CNIO Monoclonal Antibodies Core Unit

Validation

B220 PE-Cy7 RA3-6B2 #561881 BD Pharmingen. Validated in the manuscript
B220 BUV737 RA3-6B2 #564449 BD Horizon. Validated by the company and by users (cited 17 times)
CD19 PE 1D3 #557399 BD Pharmingen. Validated by the company and by users (cited 12 times)
GL7 PE GL7 #561530 BD Pharmingen. Validated by the company and by users (cited 5 times)
CD95 FITC Jo2 #561979 BD Pharmingen. Validated by the company and by users (cited 5 times)
CD138 BV421 281-2 #562610 BD Horizon. Validated by the company and by users (cited 5 times)
CD38 AF700 90 #56-0381-82 eBioscience. Validated by users (cited 6 times)
CD4 FITC GK1.5 #11-0041-81 eBioscience. Validated by users (cited 234 times)
CD4 BUV395 GK1.5 #563790 BD Horizon. Validated by the company and by users (cited 10 times)
CD8 PE 53-6.7 #553032 BD Pharmingen. Validated by users (cited 25 times)
CD11b PE-Cy7 M1/70 #561098 BD Pharmingen. Validated by the company
Gr-1 FITC RB6-8C5 #562060 BD Pharmingen. Validated in the manuscript
F4/80 APCeF780 BM8 #47-4801-80 eBioscience. Validated by the company and by isers (cited 84 times)
PRDM1 AF647 5E7 #149902 Biolegend. Validated by the company
P-S235/236-S6 AF647 D57.2.2E #4851 Cell Signaling Technology. Validated by the company and by users (cited 21 times)
IgG1 APC A85-1 #560089 BD Pharmingen. Validated by the company
CD45.1 PErCP-Cy5.5 A20 #560580 BD Pharmingen. Validated by the company and by users (cited 7 times)
CD45.2 APC-Cy7 104 #109824 Biolegend. Validated by the company and by users (cited 10 times)
CXCR5 Biotin 2G8 #551960 BD Pharmingen. Validated by users (cited 7 times)
Streptavidin PE #554061 BD Pharmingen. Validated in the manuscript
PD-1 PE-Cy7 J43 #25-9985-80 eBioscience. Validated by the company and by users (cited 16 times)
P-T389-S6K1 #9234 Cell Signaling Technology. Validated by the company and by users (cited 605 times)
S6K1 #2708 Cell Signaling Technology. Validated by the company and by users (cited 541 times)
P-T37/46-4EBP1 #2855 Cell Signaling Technology. Validated by the company and by users (cited 543 times)
4EBP1 #9644 Cell Signaling Technology. Validated by the company and by users (cited 351 times)
P-T308-AKT #2965 Cell Signaling Technology. Validated by the company and by users (cited 468 times)
P-S743-AKT #4060 Cell Signaling Technology. Validated by the company and by users (cited 2831 times)
AKT #4691 Cell Signaling Technology. Validated by the company and by users (cited 1341 times)
β-actin #A5441 Sigma. Validated by the company and by users (cited 4562 times)
IgG1 Fc-specific antibody conjugated to horseradish peroxidase # 115-035-071 Jackson Immunoresearch. Validated by users (cited 41 times)
PD-1 #84651 Cell Signaling Technology. Validated by the company
Bcl6 #AM(191E/A8) CNIO Monoclonal Antibodies Core Unit. Validated by the unit (cited 5 times).
Cleaved Caspase 3 #9661 Cell Signaling Technology. Validated by the company and by users (cited 3681 times)
PD-1 NAT105C/E3 lot num. 0208 CNIO Monoclonal Antibodies Core Unit. Validated by the unit (more than 20 citations)

Animals and other organisms

Policy information about studies involving animals; ARRIVE guidelines recommended for reporting animal research

Laboratory animals	Mus musculus, C57BL/6, males and females, from E13.5 to 1.5 year old
Wild animals	not used
Field-collected samples	no field-collected samples
Ethics oversight	Spanish National Cancer Research Center (CNIO), Instituto de Salud Carlos III (ISCIII) and Autonomous Community of Madrid (CAM)

Note that full information on the approval of the study protocol must also be provided in the manuscript.

Human research participants

Policy information about studies involving human research participants

Population characteristics	Patients included in this study were all diagnosed with follicular lymphoma (total patients with data = 44). Genotypic information on RRAGC mutation status were derived previously (Okosun et al, Nature Genetics 2016) and consists of 16 patients with RRAGC mutations and 28 patients were RRAGC wild-type.
Recruitment	The samples were compiled retrospectively from FL patients, with those with known RRAGC genotypes and available tumor biopsy blocks selected for inclusion. Relevant covariates have no known confounding effects and are not believed to significantly affect our results.

Ethics oversight	The use of patient specimens for research purposes is covered by the ethical approval obtained from the London Research Ethics Committee (LREC) of the East London and the City Health Authority (10/H0704/65 and 06/Q0605/69

Note that full information on the approval of the study protocol must also be provided in the manuscript.

Flow Cytometry

Plots

Confirm that:

☒ The axis labels state the marker and fluorochrome used (e.g. CD4-FITC).

☒ The axis scales are clearly visible. Include numbers along axes only for bottom left plot of group (a 'group' is an analysis of identical markers).

☒ All plots are contour plots with outliers or pseudocolor plots.

☒ A numerical value for number of cells or percentage (with statistics) is provided.

Methodology

Sample preparation	Mononuclear cell pools (from spleen or Bone marrow) were isolated from mouse spleens at the indicated times postimmunization. Cells were separated by crushing the spleens through a 70 micrometer mesh (Corning) in ice-cold PBS +0.1% BSA +3mM EDTA, and red blood cells were lysed using Erythrocyte Lysis Buffer (Qiagen, #79217). Cell staining was performed on ice in PBS +0.1% BSA + 3mM EDTA.
Instrument	BD Canto II, LSR-Fortessa, BD FACSAria IIu, InFlux (Cytopeia-Becton Dickinson
Software	BD FACSDiva software (BD Biosciences). FlowJo software (v 9.8.1 and v.10; TreeStar)
Cell population abundance	sorted GCB cells were >99% (B220+, CD95+, CD38-) B220+ isolated from mouse lymphoma tumors by immunomagnetic enrichment with CD45R (B220) microbeads were >90% B220 +
Gating strategy	Sorted GCB cells: singlets/live/lymph/CD19+/CD95+CD38- GCB cells were identify as singlets/live/lymph/B220+/GL7+CD95+ PC cells were identified as singlets/live/lymph/B220lowCD138+ Granulocytes were identified as singlets/Live/B220-/CD4-/CD8-/CD11b-/Gr-1+. MDSC were identified as singlets/live/B220-/CD4-/CD8-/CD11b+/Gr-1+. Myeloid cells were identified as singlets/live/B220-/CD4-/CD8-/CD11b+. Macrophages were identified as singlets/live/B220-/CD4-/CD8-/CD11blowF4-80+. T follicular helper cells (Tfh) were identified as singlets/live/B220-/CD4+/CXCR5+Foxp3-

☒ Tick this box to confirm that a figure exemplifying the gating strategy is provided in the Supplementary Information.